EYE-CLIMA
Verifying emissions of climate forcers

Carbon and greenhouse gas budgets of Europe: trends, interannual and spatial variability

DELIVERABLE 4.4

Author(s):	Philippe Ciais, Antoine Berchet

Date of submission:	27-08-2024
Version:	1.0
Responsible partner:	CNRS-LSCE
Deliverable due date:	31-10-2023
Dissemination level:	Public

Call:	HORIZON-CL5-2022-D1-02
Topic:	Climate Sciences and Responses
Project Type:	Research and Innovation Action
Lead Beneficiary:	NILU - Norsk Institutt for Luftforskning

This project has received funding from the European Union's Horizon Europe research and innovation programme under grant agreement No 101081395

Document History

Version	Date	Comment	Modifications made by
0.1	01-11-2023	First Draft	Philippe Ciais, Antoine Berchet
0.2	28-12-2023	Internal review	Rona Thompson
0.3	05-07-2024	Revised version	Philippe Ciais
1.0	27-08-2024	Submitted to Commission	Rona Thompson

This project has received funding from the European Union's Horizon Europe research and innovation programme under grant agreement No 101081395

Summary

We have performed a preliminary synthesis of European greenhouse gas (GHG) fluxes for CO_2, CH_4 and N_2O. This synthesis was a contribution to the international Regional Carbon Cycle Assessment and Processes Phase 2 (RECCAP-2) activity for Europe, coordinated by the Global Carbon Project. To access the GHG budget of Europe between 1990s and 2010s, bottom-up (BU) and top-down (TD) estimates are used and the results are compared and assessed for their spatiotemporal variability and trends. This deliverable thus consists of the descriptions of GHG (CO_2, CH_4 and N_2O) emissions estimated by different methods. This work has been published in the peer-reviewed article, Lauerwald et al. 2024. This report focuses on the contribution from EYE-CLIMA to the RECCAP-2 assessment and some text and figures in this deliverable were also used in Lauerwald et al. 2024.

In this synthesis:

- BU GHG budgets were based on a range of flux estimates for different sectors and flux components. We distinguish between direct anthropogenic emissions of GHG and the land fluxes that focus on GHG exchange between the continental biosphere and the atmosphere.
- TD global, coarsely resolved (≥2°) global inversions as well as regional inversions for Europe at a higher spatial resolution (0.5°), for a domain bounded between 15°E to 35°W and 33°N to 73°N, were used.
- TD Regional inversions may be expected to better resolve spatial patterns in GHG sources/sinks at continental scale than global inversions. Therefore, we use these regional inversions for our analysis of spatial patterns in GHG sources and sinks across Europe.
- We analyzed spatiotemporal patterns of fossil CO_2 emissions from inventories and land CO_2, CH_4, N_2O fluxes from inversions over the period 2010-2019, including local hotspots and areas with large temporal trends, based on the mean of regional inversions re-gridded to 1°. Then, we quantified interannual variability of European GHG budget in corresponding modelled period.

The results of this synthesis are used in the deliverable D5.8, the first Progress on Targets Report.

This project has received funding from the European Union's Horizon Europe research and innovation programme under grant agreement No 101081395

TABLE OF CONTENTS

This project has received funding from the European Union's Horizon Europe research and innovation programme under grant agreement No 101081395

1.Introduction

The EYECLIMA project comprehensively evaluates greenhouse gas (GHG) fluxes in Europe, including their drivers, spatiotemporal changes, and interannual variability (IAV). To ensure robust analysis, this synthesis employs both top-down (TD) and bottom-up (BU) models to calculate GHG fluxes:

1.The TD approach uses atmospheric inversion estimates.

2.The BU approach utilizes inventory-based estimates and land budget evaluations.

Initially, the budget for the most recent decade (2010-2019) is analyzed. Here we used available data from previous projects, such as VERIFY and the global CO_2 budget, and have contributed to the RECCAP2 (REgional Carbon Cycle Assessment and Processes Phase 2) initiative of the Global Carbon Project (GCP). This synthesis contains a comparison with the budgets of the previous three decades, identifying temporal trends and the sectors and fluxes responsible for these trends. Subsequently, based on regional inversion data, the spatiotemporal changes in GHG sources and sinks within Europe over the last decade are studied, with a focus on IAV, recent trends, and local hotspots of sinks and sources.

The inter-annual variability (IAV) of different GHG budgets is examined in greater detail, culminating in an assessment of the global warming potential (GWP) to explore the extent to which these fluxes are driven by climate factors.

2. Methods and Materials

2.1 GHG budgets from bottom-up estimates

To establish BU GHG budgets, we use different apporaches across various sectors and components, subsequently comparing these to the TD budget derived from inversions. We separate direct anthropogenic emissions of GHGs (Section 2.1.1 – work contributed by EYE-CLIMA) and land fluxes that focus on GHG exchanges between the continental biosphere and the atmosphere (Section 2.1.2), following guidelines proposed by Ciais et al. (2022). Our focus is on understanding how GHG sinks and sources in continental ecosystems are distributed in space and time and what is their trend over the 3 recent decades. This includes managed lands and terrestrial ecosystem-atmosphere exchange fluxes influenced by human activities. Anthropogenic emissions not related to ecosystem fluxes are categorized separately as direct anthropogenic emissions.

In cases where multiple estimates exist for a GHG sink or source, we use the median value. Additionally, we calculate lower and upper bound estimates based on either reported uncertainties in the original data, the spread of individual results from ensembles of Dynamic Global Vegetation Models (DGVMs) or inversions, or uncertainty estimates derived from expert judgment. For the latter, we adopt the relative uncertainty estimates used by Luyssaert et al. (2012) and recommended by the protocol of RECCAP 2 in Ciais et al. (2022).

2.1.1 Direct anthropogenic emissions

Direct anthropogenic emissions are split into the sectors recommended by the guidelines of IPCC (2006): Energy (F_{Energy}), industrial processes and product use (F_{IPPU}), Waste (F_{Waste}), and Agriculture, Forestry and Other Land Use (F_{AFOLU}). F_{Energy} includes emissions related to exploration, exploitation, transformation, distribution and use of fossil fuels. F_{IPPU} comprises industrial processes that release GHGs from chemical or physical transformation of materials such as during the production of steel and cement. F_{Waste} comprises all emissions related to disposal and treatment of solid waste and wastewater, including the burning of waste.

This project has received funding from the European Union's Horizon Europe research and innovation programme under grant agreement No 101081395

For the land use sector, the reported flux F_{AFOLU} comprises all anthropogenic GHG emissions and all sink removals on managed lands, where managed lands are broadly defined as ecosystems where humans intervene and over which countries claim responsibility for AFOLU fluxes (IPCC 2006). Note that national inventories in EU countries use "managed land" as a proxy for anthropogenic emissions and removals from all land, in order to avoid attempting to separate out, for example, background growth in young forests from the action of planting the forest from coincident growth acceretation due to environmental factors. Thus, F_{AFOLU} accounts for all GHG exchanges between terrestrial ecosystems and the atmosphere. F_{AFOLU} can further be split into sub-categories "Agriculture" (F_{Agri}) and "Land Use, Land-Use Change, and Forestry" (F_{LULUCF}), which facilitates the comparison of these estimates with other BU estimates focusing only on one of these two sub-categories. Soil carbon changes on agricultural land are counted as part of F_{LULUCF}, which comprises vegetation and soil carbon changes related to land-use changes and forestry, and F_{agri} includes only GHG emissions from urea applications and liming (CO_2), enteric fermentation (CH_4), manure management (CH_4, N2O), and agricultural biomass burning (CO_2, CH_4 and N2O). Note that we only consider F_{agri} as part of F_{direct} (eq. 1), while F_{LULUCF} is an anthropogenic perturbation of exchange fluxes between terrestrial ecosystems and the atmosphere (section 2.1.2). For our definition of F_{agri} as a component of direct anthropogenic emissions, we excluded N_2O emissions from agricultural soils and CO_2 emissions related to changes in soil C stocks, as those are included in the land budgets as well.

$$F_{direct} = F_{energy} + F_{IPPU} + F_{waste} + F_{agri} \text{ (eq 1)}$$

For F_{energy}, F_{IPPU}, F_{waste}, F_{agri} and F_{LULUCF}, we use several inventory global datasets that follow the definition of the sectors proposed by IPCC (2006): EDGAR v6.0, GAINS, and UNFCCC (Table 1). These data cover at least the period since 1990, and we can thus calculate consistent budgets for the three decades of the 1990s, 2000s, and 2010s. UNFCCC data are only available at national scale and are based on a collection of national GHG inventories that use national activity data and emission factors with different levels of sophistication, ranging from default emission factors (Tier 1), country- and technology-specific emission factors (Tier 2), to more complex methods that may include calibrated, process-based models (Tier 3). UNFCCC data include uncertainty estimates that take into account uncertainties in both emission factors and activity data. More information on these data can be found in Petrescu et al. (2021a, 2021b, 2023) and McGrath et al. (2023). The inventory-based estimates of EDGAR v6.0 and GAINS are spatially explicit emission based on generic activity data, but country- and technology-specific emission factors (Tier 2). For EDGAR, uncertainties were assessed by Solazzo et al. (2021). For UNFCCC data, depending on the tiers used for emission estimates in the national reporting, GHG budgets are more refined for certain countries, but not in a manner consistent across Europe. In addition, we use an ensemble of fossil-fuel CO_2 emission (F_{fossil}) estimates assembled by Andrew (2020). In agreement with that study, we consider F_{fossil} as the sum of F_{energy} and F_{IPPU} of CO_2 as in Andrew (2020). We excluded estimates based on EDGAR and UNFCCC from Andrew (2020) to avoid redundancies. Finally, we included Tier 1 estimates from FAOSTAT for F_{AFOLU}, F_{agri}, and F_{LULUCF} (Tubiello et al., 2013), and and F_{LULUCF} is used for the land budget. Those estimates are based on the global activity data from the FAOSTAT database, which are sourced from national statistical services reporting this information annually to the FAO, and from generalized emission factors proposed by the IPCC (2006).

This project has received funding from the European Union's Horizon Europe research and innovation programme under grant agreement No 101081395

Table 1: List of bottom-up datasets used in this study. The GAINS inventory and VOD data were supported by EYE-CLIMA. Other datasets are from global products as the regional datasets from EYE-CLIMA are not yet available.

Data set	Parameters, Sectors	Gases	Period	Temp. resol.	Spatial resol.
	Inventories				
UNFCCC	F_{direct} , F_{LULUCF}, ΔC_{GL}, ΔC_{CL}	CO_2, CH_4, N_2O	1990-2019	Annual	Country
GAINS	F_{direct} , F_{LULUCF}	CH_4, N_2O	1990-2015	Annual	Country
EDGAR v6.0	F_{direct} , F_{AFOLU}	CO_2, CH_4, N_2O	1970-2018	Annual	Country
FAOSTAT	F_{AFOLU}, F_{agri} , F_{LULUCF}, $F_{soil\ N2O,man}$, ΔC_{GL}, ΔC_{CL}, ΔC_{FL}	CO_2, CH_4, N_2O	1961-2019	Annual	Country
Andrew (2020)	F_{fossil}	CO_2	various	Annual	Country
FAOSTAT	$F_{wood\ harvest}$, $F_{crop\ harvest}$, $F_{wood\ trade}$, $F_{crop\ trade}$	Mass of products	1961-2019	Annual	Country
Hirschler & Oldenburg 2022	$F_{peat\ harvest}$, $F_{peat\ trade}$, $F_{peat\ use}$	Mass of products	2013-2017	none	Country
	Land surface models				
TRENDYv10	NPP, GPP, Rh,Ra,NBP	CO_2	1901-2019	Monthly	0.5°
Global N_2O budget ensemble	$F_{soil\ N2O}$	N_2O	1901-2015	Monthly	0.5°
O-CN (Zaehle et al. 2010, ext. for NMIP2)	$F_{soil\ N2O}$	N_2O	1901-2019	Monthly	0.5°
GMB2020, BU models	$F_{peat\ CH4}$	CH_4	2005-2019	Monthly	0.5°
ORCHIDEE-GMv3.2 (Chang et al. 2021)	$F_{grazing}$	C	1861-2012	Monthly	0.5°
	Other process based models				
MeMo	$F_{methanotrophy}$	CH_4	1990-2009	Monthly	1°
VPRM (Gerbig & Koch 2021)	NEE_C	CO_2	2006-2020		7.5'
	Bookkeeping models				
H&N (as in Friedling-stein et al. 2021)	F_{LUC}	CO_2	1990-2020	Annual	RECCAP2
BLUE (Ganzenmüller et al. 2022)	F_{LUC}	CO_2	1960-2019	Annual	0.25°
	Land cover data				
HILDA+	Land cover, land cover change	-	1960-2019	Annual	0.01°

This project has received funding from the European Union's Horizon Europe research and innovation programme under grant agreement No 101081395

Table 1: Continued

Data set	Parameters, Sectors	Gases	Period	Temp. resol.	Spatial resol.
	Data driven estimates				
FLUXCOM (Jung et al. 2020 BG) - RS v006	GPP, Re_{terr}	CO_2	2001-2020	Monthly	5'
FLUXCOM (Jung et al. 2020 BG) - ERA	GPP, Re_{terr}	CO_2	1990-2018	Monthly	5'
GLASS	GPP, NPP	CO_2	2001-2018	8 Day	500 m
Madani & Parazoo 2020	GPP	CO_2	1982-2016	Monthly	8 km
MODIS	NPP	CO_2	2001-2020	8 Day	500 m
BESS	GPP	CO_2	2001-2016	8 Day	1 km
Yao et al., 2020	Rh_{terr}	CO_2	1985-2013	Annual	0.5°
GFEDv4 (extended.)	F_{fire}	C	1997-2019	Monthly	0.25°
GFASv1.2	F_{fire}	C,CO_2, CH_4, N_2O	2003-2020	Daily	0.1°
Mendonca et al. (2017)	ΔC_{burial}	C		none	COSCAT
Lauerwald et al. (2023)	F_{IW}	CO_2, CH_4, N_2O	present day	none	RECCAP2
Rosentreter et al. (2023)	F_{CWa}, F_{CWL}	CO_2, CH_4, N_2O	present day	none	RECCAP2
Zscheischler et al. (2017)	$F_{weathering}$, $F_{litho2river}$, $F_{river\ export}$, ΔC_{litho}	C, CO_2	present day	none	1°
Etiope et al. (2019), updated for Petrescu et al. (2023)	F_{geo}	CH_4	present day	none	1°
EMEP	$F_{soil\ N2O,Ndep}$	N	2000-2019	Daily	0.1°
EFISCEN	ΔC_{FL}	Biomass	2000-2020	5 Year	Country
EFISCEN, gridded version	ΔC_{FL}	Biomass	2000-2020	annual	7.5'
L-VOD	ΔC_{FL}	Biomass	2011-2021	Quarterly	25 km
Byrne et al. (2023)	$F_{wood\ harvest}$, $F_{crop\ harvest}$, $F_{wood\ use}$, $F_{crop\ use}$	C	1961-2019	Annual	5'

*Spatial resolution refers to pixel size of gridded product, or to regions, which can be country areas, COSCAT regions (based on coastal segments and their catchments, Meybeck et al., 2006), or the entire study area (RECCAP2).

2.1.2 Land budgets

While we use the definitions used by the IPCC, we report the land budgets following the recommendations of Ciais et al. 2022 for RECCAP2 (Figure. 1). In general, we sub-divided the land systems further into terrestrial ecosystems (vegetation-soil systems), inland waters, and coastal ecosystems (waters and wetlands). Before we describe the land budget of each GHG further below, we describe here which flux components and data sources are shared between those budgets. The emissions from inland waters (F_{IW}), coastal waters (F_{CWa}) and coastal wetlands (F_{CWL}) are treated as shown in Fig. 1 which means that similar processes, subdivisions, and data sources are considered for each GHG. For these fluxes, we use syntheses of estimates that have been developed within the RECCAP2 initiative (Lauerwald et al., 2023 for F_{IW}; Rosentreter et al.; 2023 for F_{CWa} and F_{CWL}). All these estimates are average annual fluxes, which we assumed to be constant for the last three decades.

This project has received funding from the European Union's Horizon Europe research and innovation programme under grant agreement No 101081395

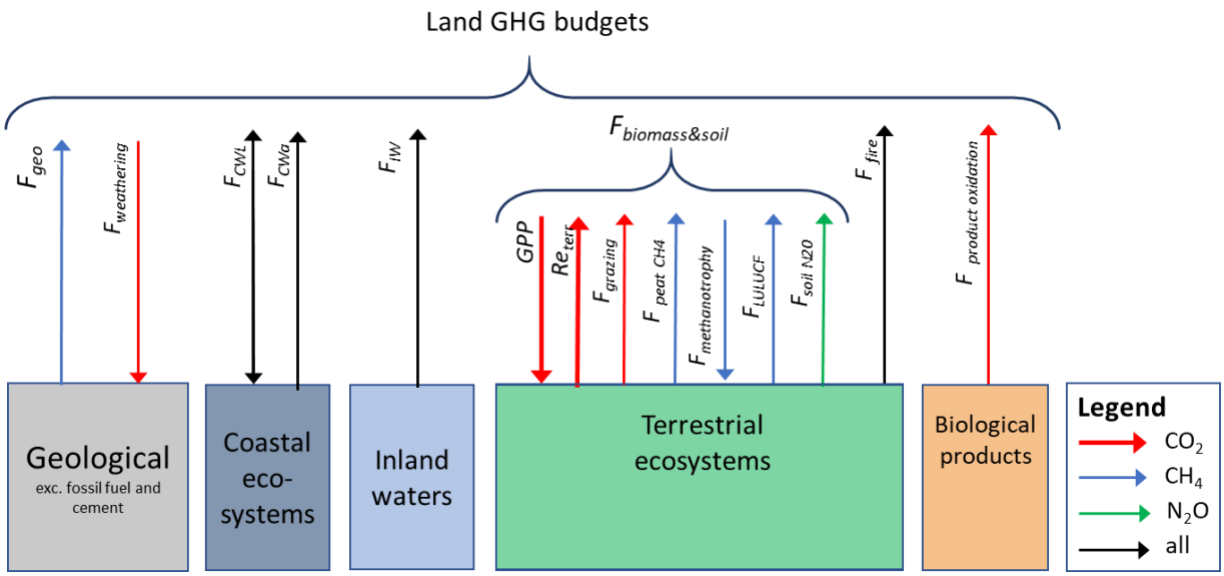

Figure 1: Greenhouse gas fluxes included for the land budget, adapted from Ciais et al. (2022) to include N_2O fluxes and coastal waters. This land GHG budget excludes direct anthropogenic emissions (see text) such as CH_4 emissions from agriculture and waste, industrial processes and fossil emissions.

Fire emissions (F_{fire}), related to in-situ burning of biomass and is distinguished from burning of waste which belongs to F_{Waste}; the burning of crop residues, which is part of F_{agri}; and the burning and decay of crop products ($F_{product\_decay}$) is a separate flux component in the CO_2 and C budgets (see below). F_{fire} is derived from two data-driven estimates: the CAMS Global Fire Assimilation System (GFAS) (Kaiser et al., 2012) and the global fire emission database (GFED) v4 (van der Werf et al. 2017). GFAS is based on fire radiative power observations from satellite-based sensors. GFAS gives emissions estimates for total C, CO_2, CH_4, CO, and N_2O. GFED is based on remotely sensed data (Moderate Resolution Imaging Spectroradiometer - MODIS and Visible Infrared Imaging Radiometer Suite - VIIRS) of fire count and burned area and emission factors based on the CASA model. GFED gives total C emissions, which we treat as equal to CO_2 emissions, but details emissions from fires of different land use types and thus permits the separation of biomass burning on agricultural land from wildfires. Both GFED and GFAS cover the last two decades. For the 1990s as no satellite data is available, we assumed that fire emissions equaled those of the 2000s. For forest disturbances losses and subsequent recovery gains a new estimate of decadal forest carbon stock loss and gain from forest disturbances is given in section 8.

The major fluxes between terrestrial ecosystems and the atmosphere are defined as detailed in the following section.

Land CO_2 budget

$$F_{land\ CO2} = GPP + Re_{terr} + F_{IW} + F_{product\ oxidation} + F_{grazing} + F_{fire} + F_{CWa} + F_{CWL} + F_{weathering} \quad \text{(Eq. 2)}$$

$$Re_{terr} = Ra + Rh \quad \text{(Eq. 3)}$$

The land CO_2 budget is the difference between gross primary production (GPP) and terrestrial ecosystem respiration Re_{terr}, which is itself the sum of autotrophic (Ra) and heterotrophic (Rh) respiration in the terrestrial biosphere (Eq. 3). CO_2 emissions from inland waters (F_{IW}) are largely fed by carbon leached from terrestrial ecosystem respiration (Battin et al., 2023), which is not included in the flux Re_{terr}. We treat emissions/uptake from coastal water (F_{CWa}) and coastal wetlands (F_{CWL}) separately as we assume that they are not included in our estimates of GPP, Ra, Rh or F_{IW}. We did not distinguish F_{LULUCF} in the land CO_2 budget of Eq. 2, as we assume this flux is included in the other fluxes in Eq. (2). F_{fire} includes

This project has received funding from the European Union's Horizon Europe research and innovation programme under grant agreement No 101081395

emissions from natural and anthropogenic fires in the landscape. For GPP and net primary production (NPP=GPP-*Ra*), we used several different estimates for the period 2010-2019 (Table 1). These include estimates from MODIS that are based on remote sensing data on leaf area index (LAI) and the fraction of photosynthetically active radiation (FPAR), from which estimates of GPP and NPP are derived in a semi-empirical way involving a light use efficiency model and gridded information on meteorological drivers as predictors (Zhao et al. 2005). We also used GPP from the Breathing Earth System Simulator (BESS, Jiang & Ryu 2016) and Mandani and Parazoo (2020) based on the same remote sensing data. Mandani and Parazoo (2020) compute GPP from a light use efficiency model that was optimized based on flux tower data and inventories (Mandani et al., 2017). BESS uses a hybrid process-based model representing the continuous exchange of carbon, water and energy between the biosphere and atmosphere. The GLASS GPP from the semi-empirical approach of Zhao et al. (2005) uses improved LAI and FPAR estimates from MODIS and AVHRR satellites.

From FLUXCOM data, we derived estimates of GPP and Re_{terr} that are upscaled from flux-tower observations from the Fluxnet network using machine learning algorithms and meteorological predictor data (Jung et al. 2020). More precisely, we used two versions of this dataset: one that was extrapolated based on remote sensing data only (RS v006), and one that was extrapolated based on both remote sensing data and meteorological forcing data (ERA5). From Yao et al. (2021), we use global estimates of annual soil heterotrophic respiration that are upscaled from 455 observed annual fluxes from the soil respiration database SRDB distributed over 290 sites based on machine learning using meteorological variables, soil moisture and other soil properties, GPP and land cover as predictors. This dataset represents an ensemble of 126 alternative estimates based on different combinations of predictor data sets. We use the mean and range of these estimates as the best estimate and uncertainty range, respectively.

For the land CO_2 budget of the 2010s, we present the median of the GPP estimates. A median Re_{terr} was derived from the two FLUXCOM estimates and the data-driven estimate as the sum of *Ra* after GLASS and *Rh* from Yao et al. (2021). For the comparison of land CO_2 budgets of the last three decades, we only used GPP and Re_{terr} from the ERA version of FLUXCOM, since it is the only dataset that covers this entire period (Table 1). Moreover, for the budget of the 2010s decade, this flux estimate was found to be close to the ensemble median of estimates described above, which further supports this choice. For comparison, we also derived the median and range of GPP, *Rh*, *Ra* and Re_{terr} for all three decades as simulated by the TRENDY v10 land surface model ensemble that were originally prepared for the Global Carbon Budget 2021 (Friedlingstein et al. 2022). We do not include TRENDY results in our budget directly, as DGVM simulations tend to be biased by the poor representation of perturbation, anthropogenic appropriation of biomass, and lateral export fluxes (Ciais et al., 2021). Moreover, we only used simulations from ORCHIDEE v2 (in the following simply referred to as ORCHIDEE), OC-N, LPJwsl, ISBA, ISAM, DLEM, CLM5, and CABLE for which the actual resolution was sufficiently high (0.5°). We excluded ORCHIDEE v3 and SDGVM models from the selection as the spatial patterns of their simulated land-atmosphere net C exchange did not correlate at all with those of the other TRENDY models.

Harvesting vegetation biomass for wood and crop products, as well as extraction of peat, increases the difference between GPP and Re_{terr}, because harvested organic matter does not feed into Re_{terr} according to our definition of that flux. The same is true for the biomass that is taken out by the grazing of livestock ($F_{grazing}$). While we assume $F_{grazing}$ to represent a flux of C instantaneously and completely returned to the atmosphere, the return of C from the use, decay or burning of wood, crop or peat products ($F_{product\ oxidation}$) is partly delayed and altered by import and export fluxes across the boundaries of our study area (Table 2 and data available as a spreadsheet from Supplementary S2 of https://agupubs.onlinelibrary.wiley.com/doi/10.1029/2024GB008141). The calculation of $F_{product\ oxidation}$ and $F_{grazing}$ is explained in detail in subsection 2.3.

This project has received funding from the European Union's Horizon Europe research and innovation programme under grant agreement No 101081395

$F_{grazing}$ is derived from a version of the ORCHIDEE model with prescribed livestock densities and simulated grassland management (Chang et al., 2021). As those simulations cover only the period 1901 to 2012, we scaled the average flux rates from the last 10 years of simulation (2003-2012) to average areas of intensively and extensively managed pastures over the period 2010-2019 derived from HILDA+ (Winkler et al. 2021). For the 1990s and 2000s, we used the results from Chang et al. (2021) directly. The atmospheric CO_2 sink related to rock weathering ($F_{weathering}$) which binds CO_2 as dissolved inorganic C which is then exported by rivers is an annual estimate from Zscheischler et al. (2017) after the empirical model developed by Hartmann et al. (2009).

Land CH_4 budget

$$F_{land}\,CH_4 = F_{peat}\,CH_4 + F_{methanotrophy} + F_{fire} + F_{IW} + F_{CWa} + F_{CWL} + F_{geo} \quad \text{(Eq. 4)}$$

For the land CH_4 budget, we separate peatland CH_4 emissions ($F_{peat}\,CH_4$) and terrestrial ecosystems with well-aerated soils, which act as CH_4 sink due to methanotrophy ($F_{methanotrophy}$) (Eq. 4). As data-driven estimates are scarce, we resorted to the diagnostic DGVM simulations as synthesized by the Global CH_4 Budget (Saunois et al., 2020) to quantify $F_{peat}\,CH_4$ and to the mechanistic methanotrophy model MeMo (Murguia-Flores et al. 2018) to quantify $F_{methanotrophy}$. Other wetlands than peat like floodplains and marshes are ignored. Note that the MeMo simulations of the CH_4 sink only cover years until 2009, and thus we had to assume the same value after that date. For the 2000s and 1990s, we used the published MeMo simulation results directly. Similarly, the DGVM results assembled for the Global CH_4 Budget allowed us to derive ensemble medians and ranges for all three decades. Finally, we include geological emissions of CH_4 (F_{geo}) from Etiope et al. (2019), which were updated for the VERIFY CH_4 and N_2O budgets (Petrescu et al. 2023). These estimates represent a climatology of average annual fluxes that do not represent interannual variability nor trends at the decadal time scale.

Land N_2O budget

$$F_{land}\,N_2O = F_{soil}\,N_2O + F_{fire} + F_{IW} + F_{CWa} + F_{CWL} \quad \text{(Eq. 5)}$$

For the land N_2O budget ($F_{land}\,N_2O$), direct soil N_2O emissions ($F_{soil}\,N_2O$) is the main flux between terrestrial ecosystems and the atmosphere (Eq. 5). We split $F_{soil}\,N_2O$ into a natural flux component $F_{soil}\,N_2O_{,nat}$, and anthropogenic flux components related to fertilizer and manure applications and residue management ($F_{soil}\,N_2O_{,man}$), as well as indirect emissions related to atmospheric deposition of reactive N ($F_{soil}\,N_2O_{,Ndep}$) which were split into emissions from agricultural ($F_{soil}\,N_2O_{,Ndep,agri}$) and other soils ($F_{soil}\,N_2O_{,Ndep,other}$). The inventory-based assessments of EDGAR and GAINS (supported by EYE CLIMA) only report $F_{soil}\,N_2O_{,Ndep,agri}$. In general, inventory-based assessments such as EDGAR, UNFCCC, and FAO (see Table 1) cover only emissions from managed lands. For natural emissions $F_{soil}\,N_2O$ and $F_{soil}\,N_2O_{,nat}$, we resorted to results from the Nitrogen Model Intercomparison Project (NMIP, Tian et al., 2019). For the estimation of N_2O emissions due to atmospheric N deposition on all soils, and on non-agricultural soils in particular, we use simulations results from the DGVM O-CN (Zaehle and Friend, 2010) as they were prepared for the second phase of NMIP, and come up with an alternative data-driven estimate using gridded data of atmospheric N deposition from the European Monitoring and Evaluation Programme (EMEP) and an emission factor of 1% following the guidance of IPCC (2019). From all these specific data sources for the land N2O budgets, we derive flux estimates for the last three decades.

2.1.3 Total GHG emissions

The budget of GHG emissions and removals is given in CO_2 equivalents (CO_2-eq.) with a global warming potential at a 100-year time horizon (GWP100) and using the conversion factors of 27 kgCO_2-eq./kg CH_4 and 273 kg CO_2-eq./kg N2O proposed by the 6th assessment report (AR6) of the IPCC (IPCC, 2021, Table 7.15). Only for F_{energy} and F_{IPPU}, we used the factor of 29.8 kgCO_2-eq./kg CH_4 proposed by the same

This project has received funding from the European Union's Horizon Europe research and innovation programme under grant agreement No 101081395

source for fossil CH_4 emissions. For the direct anthropogenic emission fluxes F_{energy}, F_{IPPU}, F_{waste} and F_{agri}, we simply summed up the estimated CO_2 equivalents for the individual GHGs. For the land GHG budget ($F_{GHG,land}$), we did the same for F_{fire}, F_{IW}, F_{CWa} and F_{CWL} (eq. 6). Then, we combined the major terrestrial vegetation and soil GHG emissions and sinks ($F_{biomass\&soil}$), which include GPP and Re_{terr} for CO_2, $F_{peat}\,CH_4$ and $F_{methanotrophy}$ for CH_4, and $F_{soil}\,N2O$ for N2O (Eq.7). Finally, we obtained $F_{land\ GHG}$ by additionally accounting for F_{geo} for CH_4 as well as $F_{weathering}$ and $F_{product\ oxidation}$ for CO_2 (Eq. 6).

$$F_{land\ GHG} = F_{fire} + F_{IW} + F_{CWa} + F_{CWL} + F_{biomass\&soil} + F_{geo} + F_{weathering} + F_{product\ oxidation} + F_{grazing} \quad \text{(Eq. 6)}$$

$$F_{biomass\&soil} = \text{GPP} + Re_{terr} + F_{peat}\,CH_4 + F_{methanotrophy} + F_{soil}\,N2O \quad \text{(Eq. 7)}$$

2.2 GHG budgets from top-down estimates

For each of the three GHGs, we use both global, coarsely resolved (≥1°) inversions as well as regional inversions for Europe at a higher spatial resolution (0.5°). As EYE-CLIMA inversions results are not yet available, we used the results from VERIFY updated for CO_2 thanks to the support of EYE-CLIMA for a domain between 15°E to 35°W and 33°N to 73°N, which does not reach the far eastern and western extents of the domain (therefore missing the eastern parts of Ukraine, and most of Greenland and Iceland). However, the excluded area represents less than 4% of the total land area and its contribution to the GHG budgets is likely low compared to the general uncertainties related to atmospheric-inversion estimates (estimates range over a factor of 2 and more). More importantly, regional inversions may be expected to better resolve spatial patterns in GHG sources/sinks at continental scale than global inversions (see Petrescu et al., 2023, Monteil et al. 2020).

For our TD CO_2 budget, we use seven global atmospheric inversions based on six inversion models (CAMS, CTE, Jena CarboScope, UoE, NISMON-CO_2, CMS-Flux), adjusted for fossil fuel emissions, that were used for the Global Carbon Budget 2021 (Friedlingstein et al., 2022;). In addition, we use four regional inversions. Three of them (Jena CarboScope Regional, PYVAR-CHIMERE, LUMIA) were used for the VERIFY European budget (McGrath et al., 2023; see this ref. for details on the inversion configurations). The fourth one is a new CIF-CHIMERE inversion, whose configuration is very close to that of the CIF-CHIMERE inversion documented in McGrath et al. (2023), but corrects in EYE-CLIMA errors and relies on a prior knowledge of the terrestrial ecosystem fluxes from a ORCHIDEE-MICT (Guimberteau et al., 2018) simulation forced with the ERA5 reanalysis meteorological data. While all of these inversions allow us to derive a TD budget representative for the decade 2010-2019, three of the global inversions further allow us to compare TD budgets for the last three decades.

For the CH_4 budget, we use the global inversions that were produced for the global methane budget GMB2020 (Saunois et al. 2020). That ensemble comprises 22 inversions, and covers the period 2000-2017, thus allowing us to derive TD budgets for the last two decades, though the second decade not being fully covered. Further, that ensemble is split into inversions based on ground based mole fraction measurements (XCH_4, 11 SURF inversions) and such based on satellite-based observations of atmospheric XCH_4 (11 GOSAT inversions). In addition, we use three regional inversions (CTE-CH_4, FLExKF, FLEXINVERT) that have been prepared and used for the VERIFY project (Petrescu et al. 2023). These estimates cover the full period 2010-2019.

For the N_2O budget, we use five global inversions that were produced and used for the global N_2O budget GN2OB2020 (Tian et al. 2020). Those inversions only cover the years 2000-2016, again allowing us to derive TD budgets for the last two decades, though the more recent decade not being fully covered. Finally, we include one regional inversion (FLEXINVERT) that was prepared and used for the VERIFY European budget (Petrescu et al. 2023) in our TD budget for 2010-2019.

2.3 Analyses of spatiotemporal patterns in GHG budgets from regional inversions

This project has received funding from the European Union's Horizon Europe research and innovation programme under grant agreement No 101081395

The analysis of spatiotemporal variability in GHG budgets from regional inversions was based on the annual net land flux for each GHG as well as for fossil CO2 emissions. The long term trend was estimated on a pixel-by-pixel basis through a linear least squares regression for the period reported. We also analysed continental and regional scale interannual variability (IAV) based on spatially-aggregated detrended fluxes for each GHG separately, as well as the IAV of the GHG net flux expressed in CO2 equivalent using GWP20 and GWP100.

To better understand IAV in GHG budgets, we followed the approach of Bastos et al. (2016) to assess anomalies in the annual budget of each GHG for specific combinations of phases of the North Atlantic Oscillation and the East Atlantic pattern. For this, we used the NAO and EA teleconnection indices calculated by NOAA CPC and available since 1950 at https://ftp.cpc.ncep.noaa.gov/wd52dg/data/indices/tele_index.nh (last access May 2021). We then calculated the boreal winter (Dec-Feb) mean values for each index, over the period 1950-2020. Given the non-stationarity of the teleconnection indices and short periods covered by our observational data, it is likely for results to be sensitive to the period considered (Li et al., 2022). For comparability of our results with those of Bastos et al. (2016), who analysed only CO2 and only global inversions, we used the upper (lower) terciles of the reference period in Bastos et al. (2016), i.e. 1982-2013 to then define positive (negative) phases of NAO and EA over the common period of 1990-2020.

We then estimate the mean GHG anomalies across all years that correspond to each NAO-EA phase combination (NAO+-EA+, NAO+EA-, NAO-EA+, NAO-EA-) for each GHG individually and also for the combined GWP20 and GWP100.

3. Bottom-up greenhouse gas budgets of Europe

This section deals with the BU budget of the three GHGs, first presented individually (sections 3.1, 3.2, and 3.3, respectively), then grouping all GHGs using the global warming potential of CH_4 and N_2O at 100 years horizon (section 3.4). The fluxes of our BU budget are presented in Figure 1. For the most recent decade of the 2010s, we listed our best estimates for these fluxes and our assessment of the level of confidence in these numbers in Table 2. We compare our BU estimates of the GHG budgets against atmospheric inversions, the value ranges of which are listed in Table 3. In addition, we reconstruct the development of GHG budgets over the last three decades, i.e. the 1990s, the 2000s and the 2010s, based on a subset of data sources that cover that time frame as completely and as consistently as possible.

This project has received funding from the European Union's Horizon Europe research and innovation programme under grant agreement No 101081395

Table 2: Best estimates for the flux components of the European GHG budget 2010-2019*. Table produced for Lauerwald et al. 2024 with a CO_2 inversion update supported by EYE-CLIMA.

	CO_2 emissions		CH_4 emissions		N_2O emissions		GWP_{100} (as CO_2 equivalents)				
Flux	Tg yr^{-1}	Conf.	Tg yr^{-1}	Conf.	Gg yr^{-1}	Conf.	Tg yr^{-1}	Conf.	CO_2	CH_4	N_2O
	Direct anthropogenic emission										
F_{energy}	3 792	***	6.66	*	108	*	4 020	***	94%	4%	1%
F_{IPPU}	321	***	0.08	*	106	--	353	**	91%	1%	8%
F_{waste}	5	*	6.37	*	52	-	191	*	3%	90%	7%
F_{agri}	11	***	10.72	**	78	*	322	***	3%	90%	7%
Total	4 130	***	23.83	*	343	*	4 867	***	85%	13%	2%
	Land budget										
GPP	-20 085	**									
Re_{terr}	16 740	**									
F_{LULUCF}			0.61	*							
$F_{peat\ CH4}$			2.00	--							
$F_{methanotrophy}$			-0.92	*							
$F_{soil\ N2O}$					906	*					
$F_{soil\&biomass}$	-3 345	*	1.69	--	906	*	-3 052	**	110%	-1%	-8%
$F_{grazing}$	484	*					484	*			
$F_{product\ oxidation}$	1 241	**					1 241	**			
$F_{weathering}$	-42	*					-42	*			
F_{geo}			2.50	**			68	-			
F_{fire}	34	*	0.06	*	3.2	*	36	*	93%	4%	2%
F_{IW}	191	*	4.10	*	17	-	306	*	62%	36%	2%
F_{CWa}	25	*	0.01	-	4.8	*	27	*	94%	1%	5%
F_{CWL}	-15	-	0.01	-	-0.2	--	-15	-	101%	-2%	0%
Total	-1 426	*	8.37	-	930	*	-946	-	151%	-24%	-27%

*The global warming potential at the 100-year horizon (GWP_{100}) is calculated based on IPCC AR6. We assign different level of confidence to our estimates: very high: ±10% (***), high: ±25% (**), moderate: ±50% (*), low: ±100% (-), and very low (--).

This project has received funding from the European Union's Horizon Europe research and innovation programme under grant agreement No 101081395

Table 3: Comparison of our bottom-up land GHG budgets against top-down estimates from atmospheric inversions. Table produced for Lauerwald et al. 2024 with a CO_2 inversion update supported by EYE-CLIMA.

Part of GHG budget assessed	Method of assessment	Estimated flux in Tg CO_2 yr^{-1}, Tg CH_4 yr^{-1}, or Gg N_2O yr^{-1}		
		Best estimate	Lower estimate	Upper estimate
CO_2 budget				
Land budget	Bottom up, eq. 2	-1 426		
	Global inversions	-958	-634	3443
	Regional inversions	-743	-1013	-593
CH_4 budget				
Total budget	Bottom up	32		
	Global inversions, surface observations	32	22	39
	Global inversions, satellite based	28	25	37
	Regional inversions	36	33	44
Land budget, minus (F_{fire} +F_{geo})	Bottom up	6		
	Regional inversion (CTECH4)	4		
$F_{peat\ CH4}$	Bottom up	2.0	0.6	3.3
	Global inversions, surface observations	2.0	1.7	8.4
	Global inversions, satellite based	2.1	1.7	4.9
N_2O budget				
F_{total}	Bottom up	1 274		
	Global inversions	1 472	682	1 594
	Regional inversion (Flexinvert)	1 331		

3.1. CO_2

Direct anthropogenic emissions, which do not include F_{LULUCF} dominate the CO_2 budget, and amount to an average emission of 4.1 Pg CO_2 yr^{-1} over 2010-2019 (Table 2). The largest contribution (~90%) is from F_{Energy} while F_{IPPU} (8%), F_{Agri} and F_{Waste} are minor. There is a high level of confidence in these estimates.

For the land CO_2 budget, our BU estimate gives a net sink of 1.4 Pg CO_2 yr^{-1} over 2010-2019, which offsets one third of the direct anthropogenic emissions (Table 2). We assign a moderate level of confidence (±50%) to this estimate. The BU estimate is in the range of global atmospheric inversions, but a stronger sink than the regional inversions, including the one updated in EYE-CLIMA (Table 3). The land CO_2 budget is dominated by the difference between gross primary production (GPP) and net ecosystem respiration of terrestrial ecosystems (Re_{terr}), which is 3.3 Pg CO_2 yr^{-1}. While we have a high level of confidence (i.e. ±25%) in *GPP* and Re_{terr} estimates, the difference between these fluxes is

This project has received funding from the European Union's Horizon Europe research and innovation programme under grant agreement No 101081395

uncertain and was given moderate level of confidence (±50%). This difference is due to the anthropogenic appropriation of biomass through the harvest and use of wood and crop products, which does not feed into the ecosystem respiration (see Ciais et al., 2021). This harvested carbon is returned to the atmosphere through the oxidation of the products, which we estimate at ~1.3 Pg CO_2 yr^{-1} with a high level of confidence (±25%). Another ~0.5 Pg CO_2 yr^{-1} is returned from biomass to the atmosphere through grazing by livestock. Inland water emissions add 0.2 Pg CO_2 yr^{-1}. Emissions from coastal waters and wildfires are minor land sources of CO_2 to the atmosphere. Rock weathering and coastal wetlands are very small sinks of CO_2.

Overall, the total BU CO_2 budget gives a net source of ~2.7 Pg CO_2 yr^{-1} for the 2010s. Using the smaller selection of data sources of the different flux components that were available for the last three decades, the net source for the 2010s is slightly higher with ~2.9 Pg CO_2 yr^{-1} (Figure 3). For a consistent analysis of the three decades, GPP and Re_{terr} are taken solely from FLUXCOM ERA5 dataset.

Figure 2 gives the total CO_2 budget for the last three decades as well as changes in component fluxes. F_{IW}, F_{CWa}, F_{CWL}, and $F_{weathering}$ are assumed to remain constant across the three decades in absence of varying estimates. We also had to assume that F_{fire} did not change between the 1990s and the 2000s.

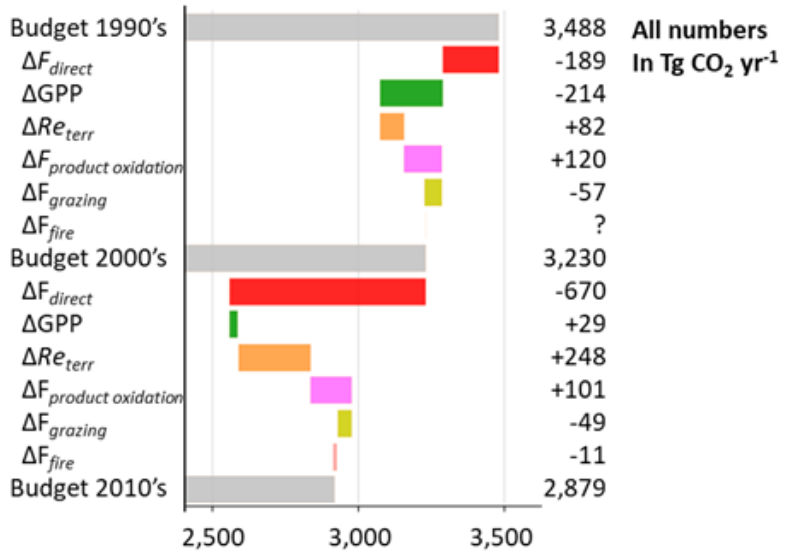

Figure 2: Evolution of European CO_2 budget over the last three decades. Note that there is no estimate for F_{fire} in the 1990s. This figure is reproduced from Lauerwald et al. 2024.

The data in Figure 2 show that that the net CO_2 source has notably decreased from the 1990s to the 2000s and further to the 2010s. For the 2000s, our estimate of 3,230 Tg CO_2 yr^{-1} is quite close to Luyssaert et al. (2012) of ~3,270 Tg CO_2 yr^{-1} for RECCAP1. However, RECCAP1 excluded Ukraine, Belarus, and Rep. of Moldova. From the 1990s to the 2000s, the reduction in the net source of 258 Tg CO_2 yr^{-1} is due to reductions in F_{direct}. However, 69 Tg CO_2 yr^{-1} are still due to an increase in the land CO_2 sink. Between these two decades, we find an important increase in average GPP which is only partly offset by an increase in Re_{terr}. We further find an increase in $F_{product\ oxidation}$ and a decrease in $F_{grazing}$.

From the 2000s to the 2010s, the reduction in F_{direct} is about 3.5 times as strong as between the 1990s and 2000s as shown by(McGrath et al., 2023; Petrescu et al., 2021a). However, this reduction in direct anthropogenic emissions was partly offset by a reduction in the land CO_2 sink of 318 Tg CO_2 yr^{-1} (Figure 3). From the 2000s to the 2010s, even if GPP slightly decreased, it was accompanied by a strong

This project has received funding from the European Union's Horizon Europe research and innovation programme under grant agreement No 101081395

increase in Re_{terr} that is three times higher than that between the 1990s and the 2000s. Changes in $F_{grazing}$ and $F_{product\ oxidation}$ are comparable to that between the 1990s and the 2000s, with a similar increase in emissions from anthropogenically appropriated biomass back to the atmosphere of 52 Tg CO_2 yr^{-1}. Being generally a minor flux in the European CO_2 budget (Tables 3), also changes in F_{fire} have only a small influence on decadal trends in the CO_2 budget (Figure 3).

Overall, according to our BU assessment, the land CO_2 sink decreased from 1.5 Pg CO_2 yr^{-1} in the 1990s to 1.3 Pg CO_2 yr^{-1} in the 2010s. This is comparable to the TD estimates that give a decrease from 1.3 (0.3–1.5) Pg CO_2 yr^{-1} to 1.0 (0.0–1.5) Pg CO_2 yr^{-1}, respectively (ensemble median and range). For the 2000s, however, our BU estimate diverges substantially from inversions, with 1.6 Pg CO_2 yr^{-1} vs 0.9 (0.1–1.2) Pg CO_2 yr^{-1}, respectively.

3.2. CH_4

For 2010-2019, our BU estimates of CH_4 net emissions is of ~32 Tg CH_4 yr^{-1} with a moderate level of confidence (up to ±50%). This BU estimate lies within the range of TD estimates by Saunois et al. (2020), based on surface observations (22 to 39 Tg CH_4 yr^{-1}, median of 32 Tg CH_4 yr^{-1}) or GOSAT satellite data (25 to 37 Tg CH_4 yr^{-1}, median of 28 Tg CH_4 yr^{-1}, Table 3). In contrast, our BU estimate is lower than in regional inversions (33 to 44 Tg CH_4 yr^{-1}, Table 3). About three quarters of European CH_4 emissions, i.e. ~24 Tg CH_4 yr^{-1} is from the sum of direct anthropogenic emissions F_{energy}, F_{IPPU}, F_{waste}, and F_{agri}. With ~11 Tg CH_4 yr^{-1}, the agricultural sector contributes nearly half of direct emissions. With 6 to 7 Tg CH_4 yr^{-1}, the energy and the waste sector are smaller emitters, while contribution of the industrial production and product use sector is small.

About one quarter of CH_4 emissions is attributed to natural sources in Europe, yet with a low level of confidence to our BU estimate of the land CH_4 budget. The largest sources in our land CH_4 budget are inland waters and geological emissions with 4.1 and 2.5 Tg CH_4 yr^{-1}, with moderate (±50%) and high (±25%) levels of confidence (Table 2). Peatland emissions are smaller and poorly constrained (range of 0.6 to 3.3 Tg CH_4 yr^{-1}). Emissions from fires, coastal waters and coastal wetlands do not play a significant role.

When comparing the CH_4 emissions for the 1990s, 2000s and 2010s, the BU approach gives a strong decrease in the overall net sources (Figure 3). Splitting changes in F_{direct} into changes in F_{agri} , F_{energy}, F_{IPPU}, and F_{waste}, from the 1990s to the 2010s, shows the net source decreased by about one quarter, mainly due to reductions in F_{energy}, F_{IPPU}, and F_{waste}. Changes in natural sinks and sources are small. No temporal estimate is available for inland water emissions.

This project has received funding from the European Union's Horizon Europe research and innovation programme under grant agreement No 101081395

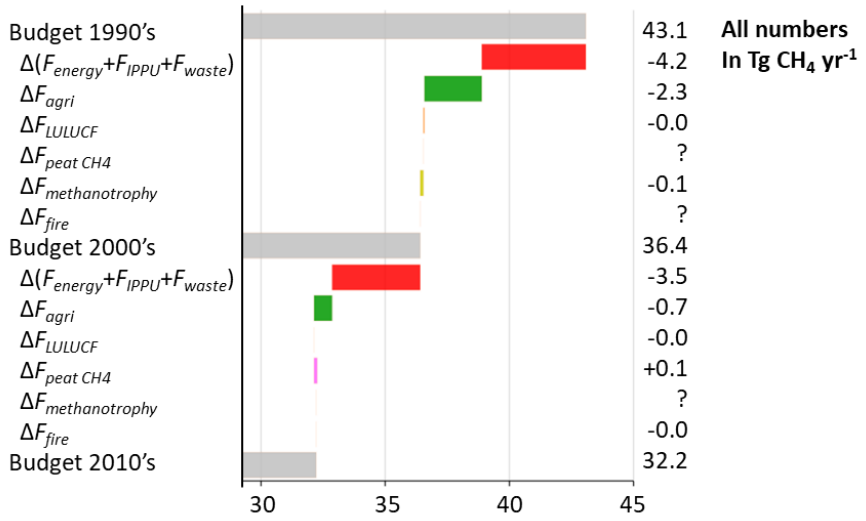

Figure 3: Evolution of European CH_4 budget over the last three decades. Note that there is no estimate for F_{fire} in the 1990s. This figure is reproduced from Lauerwald et al. 2024.

The CH_4 BU emission estimate of 36 Tg CH_4 yr^{-1} for the 2000s is higher than the RECCAP1 estimate of 28 Tg CH_4 yr^{-1} by Luyssaert et al. (2012) for 2001-2005 who excluded Republic of Moldova, Ukraine and Belarus. Petrescu et al. (2023) found a decrease in direct emissions by 16.5%, mainly due to reductions in F_{waste} (-10.1%) and F_{energy} (-4.4%) comparable to our study. However, global inversions, do not show a trend from the 2000s to 2010s, with a rather constant net source of ≈32 Tg CH_4 yr^{-1}.

3.3. N_2O

For the European N_2O budget 2010-2019 based on Lauerwald et al. as we do not have new estimates from EYE-CLIMA, our BU estimated emission is ~1.3 Tg N_2O yr^{-1} with a moderate level (±50%) of confidence. The BU estimate is within the range of TD estimates from Tian et al. (2020) (0.7 to 1.6 Tg N2O yr^{-1}, median of 1.5 Tg N_2O yr^{-1}), and close to the regional TD estimate from Flexinvert used by Petrescu et al. (2023) (1.3 Tg N_2O yr^{-1}, Table 3). We attribute only about one quarter of emissions to F_{direct}, to which all four flux components, i.e. F_{energy}, F_{IPPU}, F_{waste}, and F_{agri}, contribute substantially. For F_{agri}, we only include emissions from manure management and biomass burning. Emissions due to fertilizer and manure application as well as residue management are put together as the soil management flux $F_{soil}N_2O_{,man}$ part of $F_{soil}N_2O$, and thus of the land N_2O budget, which is reported separately from F_{direct}.

The different inventories have similar estimates for F_{energy} and F_{agri} with a moderate level of confidence. For F_{IPPU}, we are less confident, because inventory based estimates range from 58 Gg N_2O yr^{-1} (UNFCCC) to 210 Gg N_2O yr^{-1} (EDGAR). Similarly, we assign a low level of confidence to F_{waste} for which estimates range from 42 Gg N_2O yr^{-1} (UNFCCC) to 76 Gg N_2O yr^{-1} (GAINS). GAINS will be updated in EYE-CLIMA.

The land N_2O budget accounting for three quarters of the total emissions, is dominated by soil N_2O emissions ($FN_2O_{,soil}$, about 97% of the land N_2O budget with a 'moderate' level of confidence and a mean value of ~0.93 Tg N_2O yr^{-1}. 0.68 Tg N2O yr^{-1} of $FN_2O_{,soil}$ can be attributed to $F_{soil}N_2O_{,man}$, while atmospheric deposition of reactive N ($F_{soil}N_2O_{,Ndep}$) accounts for 0.07 Tg N2O yr^{-1} of soil indirect emissions, and the remaining 0.17 Tg N2O yr^{-1} can be attributed to natural background emissions $FN_2O_{,soil,nat}$. The emissions from inland and coastal waters are small (Table 2). Note further that these fluxes are not fully natural. In Europe, about two thirds of inland water emissions can be attributed to anthropogenic N inputs from fertilizer, manure and sewage water (Petrescu et al., 2023 based on Yao et al., 2020).

This project has received funding from the European Union's Horizon Europe research and innovation programme under grant agreement No 101081395

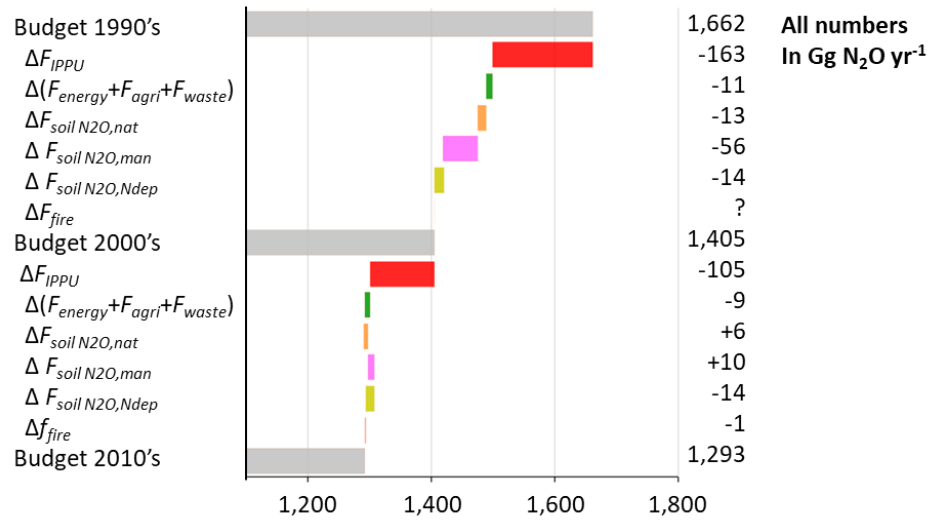

Figure 4: Evolution of European N2O budget over the last three decades. Note that there is no estimate for F_{fire} in the 1990s. This figure is reproduced from Lauerwald et al. 2024

Figure 4 shows decadal N_2O budgets since the 1990s, including the sectors which changed. From the 1990s to the 2010s, total emissions of N_2O decreased by about one fifth, due to reductions in F_{IPPU}. From the 2000s to the 2010s, the decrease in BU emissions is consistent with TD budgets from 1.6 (0.9-1.7) Tg N2O yr^{-1} to 1.5 (0.6-1.6) Tg N_2O yr^{-1} , respectively, derived from global inversions In contrast, F_{energy}, F_{waste}, and F_{agri} remained relatively constant. We found a large spread in different estimates of F_{IPPU} but all inventories show a strong decline over the three decades (UNFCCC, EDGAR, GAINS), from 141 Gg N_2O yr^{-1} (EDGAR) to 339 Gg N_2O yr^{-1} (GAINS). Interestingly, for the 2000s, the spread between these three inventory-based estimates is quite low, with estimates ranging from 210 to 226 Gg N_2O yr^{-1} only. For the 1990s and the 2010s there is a much more pronounced spread between the different data sources that explains the difference in flux changes over the three decades between the different estimates. Despite the large uncertainties related to F_{IPPU}, we can conclude that reductions in this flux are the most important driver behind reduction in total N_2O emissions.

From the 1990s to the 2000s, there was a notable reduction in $F_{soil}N_2O_{,man}$, followed by a slight increase to the 2010s. EDGAR and FAO agree on this trend. For $F_{soil}N_2O_{,Ndep}$, we derived a continuously-decreasing trend from 99 Gg N_2O yr^{-1} in the 1990s to 71 Gg N_2O yr^{-1} in the 2010s based on EMEP data, the only data source that covers all soils. EMEP estimates for agricultural soil only ($F_{soil}N_2O_{,Ndep,agri}$), has similar trends and flux sizes from GAINS and EDGAR. In contrast, simulations with O-CN give $F_{soil}N_2O_{,Ndep}$ that increase from 106 Gg N_2O yr^{-1} in the 1990s to 135 Gg N_2O yr^{-1} in the 2010s. This may be explained by the fact that with this model, $F_{soil}N_2O_{,Ndep}$ is calculated as difference between simulations with and without atmospheric deposition of N, and thus accounts also for indirect effects on N_2O emissions through fertilizing effects and accumulation of N in biomass, litter and soil organic matter. Depending on the residence time in these organic N pools, a historically increased N-deposition may have a certain legacy effect on N_2O emissions. In contrast, the EF-based methods account only for N_2O emissions from direct (de-)nitrification of deposited reactive N itself, and thus only accounts for the instantaneous effect of deposition on N_2O emissions. Overall, for $FN_2O_{,soil}$, i.e. the sum of $F_{soil}N_2O_{,man}$, $F_{soil}N_2O_{,Ndep}$ and the natural background flux $FN_2O_{,soil,nat}$, and largest source of N_2O, our BU assessment gives a slight decrease from the 1990s to 2000s, but there is no notable trend between the 2000s and the 2010s. That agrees with Tian et al. (2020), who did not find a notable trend in soil N_2O emissions for Europe over the last two decades. The decrease from the 1990s to the 2000s may be explained by the EU nitrate directive which

This project has received funding from the European Union's Horizon Europe research and innovation programme under grant agreement No 101081395

has led to a decrease of manure and fertilizer application during the 2000s, which may have led to a subsequent decrease in N_2O emissions (Velthof et al., 2014).

3.4. All GHGs

When we combine the three GHGs for the decade of the 2010s, we obtain a total CO_2-equivalent emission of 4.87 Pg CO_2-eq. yr^{-1} for direct anthropogenic emissions. For the land budget, we obtain a net sink of -0.92 Pg CO_2-eq. yr^{-1}. However, while we have a high level of confidence in the estimated direct emissions, our level of confidence in the land budget is rather low (Table 2 from Lauerwald et al. 2024). F_{energy} contributes ~80% to direct anthropogenic emissions. CO_2 dominates the CO_2-eq. emissions of both F_{energy} and F_{IPPU} (>90%, Table 2). In contrast, CH_4 dominates the CO_2-eq. emissions of F_{waste} and F_{agri} (~90% in each case).

The land GHG budget is dominated by the strong land CO_2 sink, of which only one third is counterbalanced by net CH_4 and N_2O emissions. In contrast, Tian et al. (2016) found the European land budget to be a net-source of GHG based on a BU assessment, while a TD assessment showed the budgets to be close to neutral with a huge range of uncertainties. As most important flux components, the net-exchange between plant biomass, vegetation and atmosphere ($F_{soil+biomass}$), as well as the oxidation of harvested products ($F_{product\ oxidation}$) are dominated by CO_2. However, as these fluxes partly balance each other, the overall dominance of CO_2 in the land GHG budget diminished. As a component of the final net land GHG sink of -0.92 Pg CO_2-eq. yr^{-1}, the inland water emissions of 0.31 Pg CO_2-eq. yr^{-1} become an important flux component. While ~62% of F_{IW} are attributed to CO_2, CH_4 has a sizable contribution of 36%, which demonstrates the significant role of this GHG in the land budget. The contribution of N2O in F_{IW} is nearly negligible. Moreover, the weight of N_2O emissions in the land GHG budget is largely due to soil emissions, of which the major proportion represents anthropogenic perturbations through management and atmospheric deposition of reactive nitrogen.

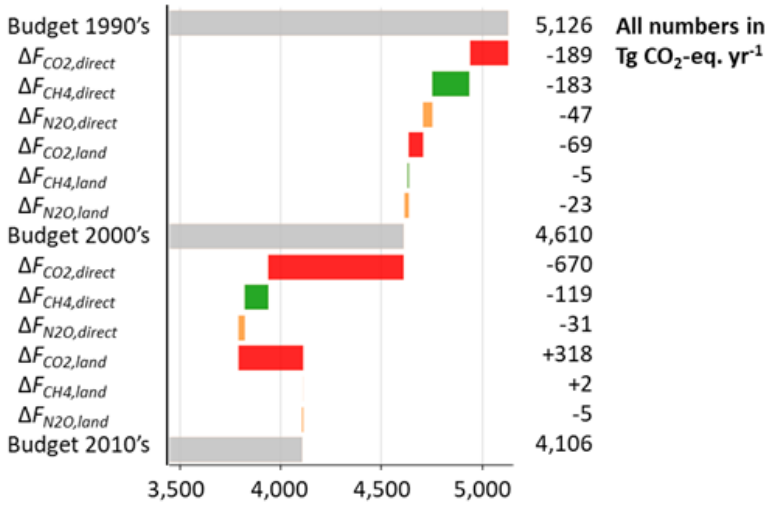

Figure 5: Evolution of European greenhouse gas budget over the last three decades, reported in CO_2 equivalent using GWP100 to convert CH_4 and N_2O into CO_2 equivalent. This figure is reproduced from Lauerwald et al. 2024.

Figure 5 shows the evolution of the European GHG budget over the last three decades. The Figure further lists how changes in direct emissions versus changes of the land budgets of the three GHGs contributed to the changes in the GHG budgets between the three decades. Note that for the last decade, the net-emissions here are slightly higher than reported in Table 2, mainly following the lower land CO_2 sink resulting from a narrower selection of datasets covering better the three decades (see section 2.1.2). From the 1990s to the 2010s, net emissions decreased by nearly one fourth. From the 1990s to

This project has received funding from the European Union's Horizon Europe research and innovation programme under grant agreement No 101081395

2000s, this decrease amounted to ~0.5 Pg CO_2-eq. yr^{-1}, of which about two thirds were due to reductions in direct emissions of CH_4 and CO_2. From the 2000s to the 2010s, net emissions decreased by another ~0.5 Pg CO_2-eq. yr^{-1}, which was mainly due to net decrease in direct CO_2 emissions of similar size. From the 1990s to the 2000s, the strength in the land CO_2 sink slightly increased, whilst it decreased from the 2000s to the 2010s, largely off-setting the effect of reduced direct emissions of the other two GHGs CH_4 and N_2O. Changes in the land budgets of CH_4 and N_2O are small compared to those in other sectors.

4. Spatiotemporal patterns in GHG budgets from regional inversions

In this section, we analyze spatiotemporal patterns of fossil CO_2 emissions and land CO_2, CH_4, N_2O fluxes over the period 2010-2019, including local hotspots and areas with large temporal trends, based on the mean of regional inversions re-gridded to 1°.

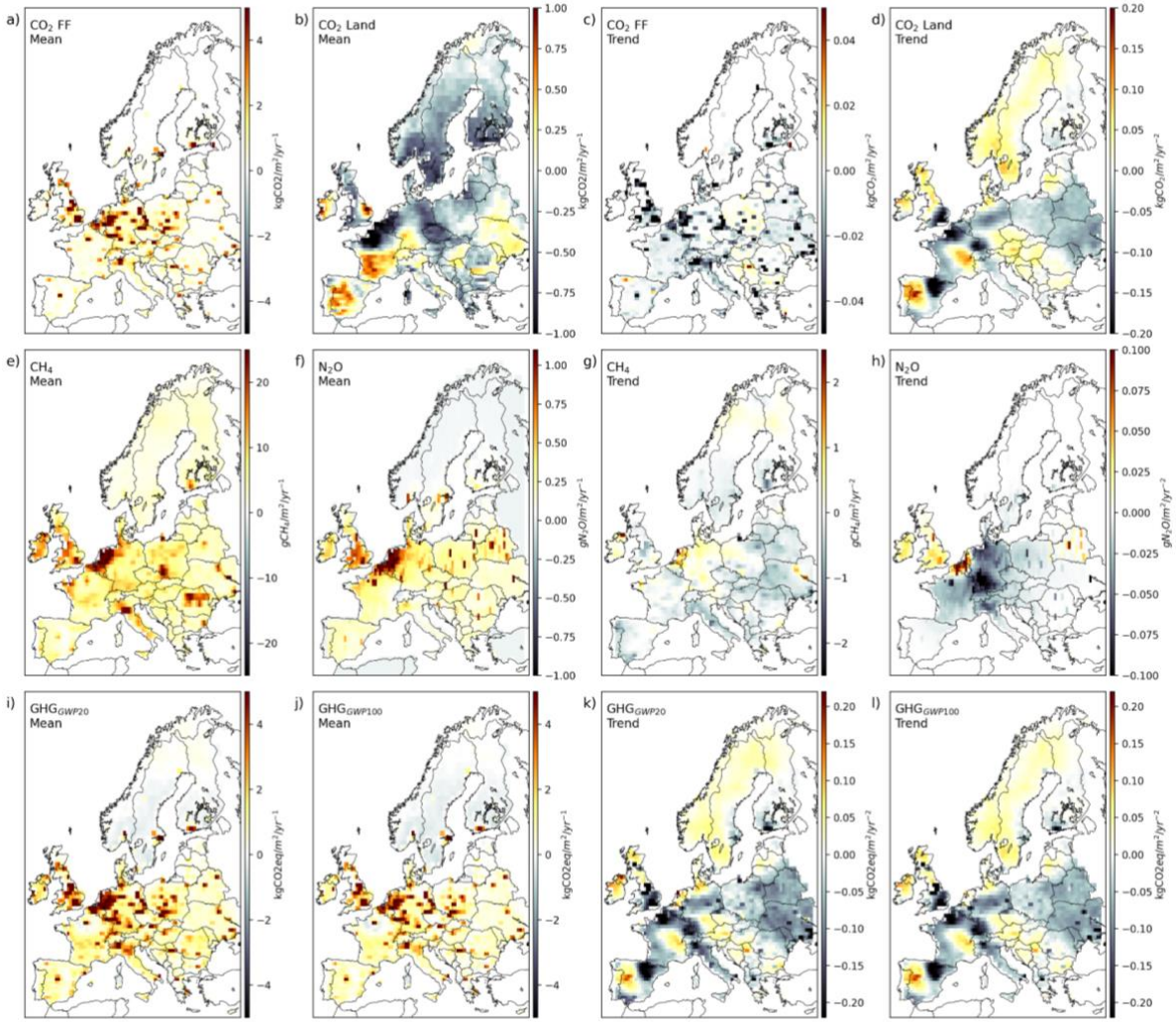

Figure 6. Spatial patterns in GHG budgets from regional inversions for the period 2010-2019: prescribed fossil CO_2 emissions (a, c), land CO_2 fluxes (b, d), CH_4 emissions (e, g), N_2O emissions (f, h), and net GHG balance combining the three GHGs at a 20 year (i, k) and 100 year (j, l) horizon. Left two columns are the means, right two columns are the trends. This figure is reproduced from Lauerwald et al. 2024.

4.1 Fossil CO_2 emissions

The spatial distribution and trend of fossil CO_2 emissions prescribed to regional inversions (i.e. not optimized) are shown in Figure. 6a,c. These priors were derived from EDGAR v4.3, BP statistics, and

This project has received funding from the European Union's Horizon Europe research and innovation programme under grant agreement No 101081395

satellite measurements of atmospheric concentration of NO_2 as important co-emittent of CO_2 in fossil fuel combustion, while the spatial disaggregation is entirely based on EDGAR v4.3 and is representative for the year 2010 (see McGrath et al., 2023 for details). Emissions are concentrated over densely populated areas in the UK, Benelux, Italy's Po Valley with emission rates higher than 6 $kgCO_2\ m^{-2}\ yr^{-1}$ over 1º grid cells, and in megacities and point sources such as power plants and industrial sites. In total, 80% of emissions are located over 23% of the land area when spatial resolution is smoothed to 1° degree like in Figure 6a,c.

Following the numbers assembled by the Global Carbon Atlas (https://globalcarbonatlas.org/, accessed on 2024-01-02) based on Friedlingstein et al. (2022), fossil CO_2 emissions have been going down in Europe since 1990, with an average rate of decrease of -1.5 % yr^{-1}. Emission reductions rates differ between countries with the largest reduction rates being in the UK (-2.8% yr^{-1}), Italy (-2.2% yr^{-1}), intermediate values in France (-1.6% yr^{-1}) and Germany (-1.5% yr^{-1}), Spain (-1.1% yr^{-1}) and in former eastern block countries excluding Poland (-1.2% yr^{-1}). In Poland, emissions decreased only by -0.2 % yr^{-1}. Note however that the map of emission trends in Figure. 6c has grid cells with increasing emissions, highlighting that some sectors have continued to increase emissions.

Since 1990, fossil CO_2 emissions have been going down by -1.1 % yr^{-1} in the EU27 and -1.5 % yr^{-1} in Europe (excluding Russia). Coal emissions showed the fastest decrease by -3.2 % yr^{-1} in the EU27 and -2.6 % yr^{-1} in Europe. Emissions from oil show a smaller decrease (-0.8 % yr^{-1} in EU27) while those from natural gas decreased to a minimum in 2015 and increased again, resulting in an average trend of -0.9 % yr^{-1} during 2010-2019. Emissions reductions rates differ between countries, the largest reduction rates being in the UK (-2.8% yr^{-1}), Italy (-2.2% yr^{-1}), intermediate values in France (-1.6% yr^{-1}) and Germany (-1.5 % yr^{-1}), Spain (-1.1 % yr^{-1}) and in former eastern bloc countries excluding Poland (-1.2 % yr^{-1}). In Poland, emissions decreased only by -0.2 % yr^{-1}. In total 90% of the EU27 emission's reduction originated from the five largest economies (Germany, France, UK, Italy, Spain, Poland) which altogether represent 80% of the mean EU27 emission. Note that the map of emission trends in Figure 6c) has grid cells with increasing emissions, as some sectors have continued to increase emissions.

Importantly, the spatial activity data for the year ≈ 2015 used for the GRIDFed emission map underlying the trend patterns Figure 6c) are not updated each year, so that the annual national fossil CO_2 emission reduction is spatially distributed in proportion to emissions from each grid cell. Therefore, the grid cells containing coal plants that closed during the period do not show up with a huge local reduction of emission in Figure 6c). Typically a large plant (~1000 MW) emits 5 Mt $CO_2\ yr^{-1}$, equivalent to the emissions from a 300,000 people city in Europe (Moran et al., 2022). In 2016, only the UK, Belgium and Sweden announced a phase out of coal in power generation for 2030, whereas in 2022 more than than 12 countries committed to it and 10 others did phase out coal. It is therefore important for the fossil emission map prescribed to inversions to be up to date for the location of disappearing (or appearing) point sources, as shown in Figure 7. Because emissions of power plants which do not exist anymore were wrongly prescribed to atmospheric transport models, all regional inversions likely compensated by adding an increasing land CO_2 sink around decommissioned plants, which biases the patterns of their land CO_2 sink and its trends, making a comparison to bottom-up estimates virtually impossible over many regions where coal power plants have closed.

This project has received funding from the European Union's Horizon Europe research and innovation programme under grant agreement No 101081395

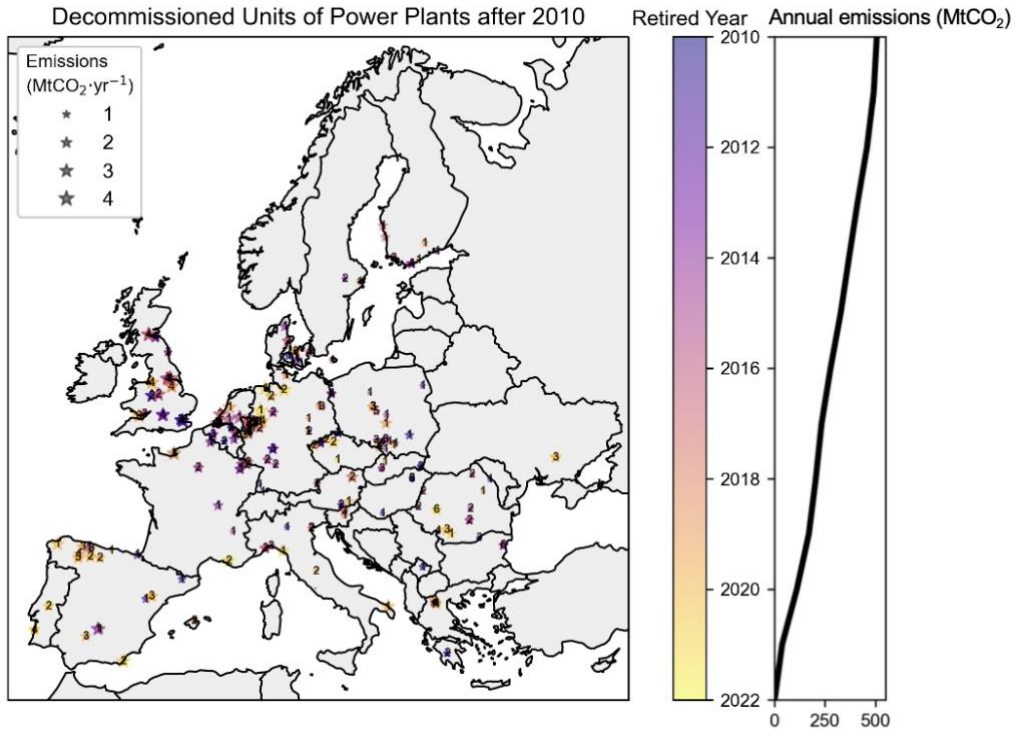

Figure 7. Location of the coal power plants that closed in Europe between 2010 and 2022. The magnitude of the emission prior closure is indicated by the size of each star symbol and the year of closure by the color palette. The right hand plot shows the reduction of corresponding CO_2 emissions since 2010, with a total reduction of 500 $MtCO_2$ by 2022. This figure is reproduced from Lauerwald et al. 2024.

4.2 Land CO_2 budget

Figure 6b shows the mean annual net CO_2 land flux excluding fossil CO_2 emissions, as estimated by the mean of regional inversions. The range of the corresponding sinks and sources (negative and positive values) at 1° spatial resolution is three times smaller than the one of fossil CO_2 emissions. According to the mean of regional inversions, most European countries are net CO_2 sinks except Spain, southern UK, southern France and Ukraine. The trend of the land CO_2 sink shows different patterns than the mean value. We verified that the trend of inversions is not given by the trend of their prior land flux. The trend of the prior shows a decreasing CO_2 sink where the trend of inversions shows regions with strong increases (north of France, north of Spain). There are however also large areas where both priors and inversions show strong decreases of the land CO_2 sink (in UK, from Southern Germany to Czech Republic, and in Scandinavia). Interestingly, regions that are weak sinks in the mean flux of inversions (northern Spain in Figure 6) show the largest sink increase over time. There is no evidence for 'favorable' trends in climate driving increased plant growth, nor for shifts in land use (such as decreased harvest) in these two regions. The trend of weakening CO_2 sinks in Scandinavia is possibly linked to changes in forest management and the cutting of old forests (Ahlström et al., 2022). On the other hand, Poland and Eastern European countries show a strong CO_2 sink that intensified over time, which may be explained by a substantial increase in forest biomass (Winkler et al., 2023).

4.3 CH_4 emissions

The CH_4 emissions from the mean of regional inversions shown in Figure 6 with anthropogenic and natural emissions. Fossil fuel extraction in Europe is limited mainly to gas extraction in the Netherlands, the North Sea (offshore), and Romania, as well as coal mining in Poland. CH_4 emissions are more diffuse but present high values in agricultural and populated areas (landfills) and in coal mining basins (e.g. the

This project has received funding from the European Union's Horizon Europe research and innovation programme under grant agreement No 101081395

Silesia region of Poland). There are few hotspot regions of CH_4 emissions with emission rates exceeding 0.01 kg CH_4 m^{-2} yr^{-1}, namely in the UK, Benelux and Western Germany, Southern Poland and Italy's Po Valley. These high emissions rates are mainly associated with CH_4 emissions from agricultural activities (e.g., cattle farming (enteric fermentation) and rice cultivation). According to UNFCCC 2022 official inventories submissions, these regions/countries are in the top ten of the CH_4 agricultural emitters, responsible for 70 % of the total CH_4 emissions in the EU27+UK. Following the same sources, emission rates in Belarus and Ukraine are lower on average than in EU27+UK. Note that the regional inversions are constrained by atmospheric observations over Western Europe, but not over Eastern Europe where their solution is close to the prior inventory (Petrescu et al., 2023). This may further explain why with regard to average emissions, global inversions tend to be better in agreement with bottom-up estimates than the regional inversions (see Table 3).

Deng et al. (2022) used global CH_4 inversions from Saunois et al. (2020) updated until 2017, which have a coarser spatial resolution than the three regional inversions used in this study. They found a consistent decreasing trend in inventories and inversions for the EU27 over the period 2000-2017, including both GOSAT-based and surface station-based inversions. Here, from regional inversions limited to a shorter period in 2010-2019 that will be updated in EYE-CLIMA, the spatial distribution of the CH_4 emissions trend suggests large decreases in Belarus and Ukraine, no strong increase in Poland (unlike in the prior) and an increase in Benelux countries, Germany, Ireland, Western France and Scandinavia. The trend of CH_4 emissions from regional inversions is therefore different from the trend of the prior (EDGARv4.2), which shows a small decrease across all European countries and large increases in Ireland and Poland.

4.4 N_2O emissions

Anthropogenic and natural N_2O emissions from inversions include industrial emissions (point sources) from the production of chemicals and other emissions (diffuse) mainly from agriculture. The map of N_2O emissions optimized by regional inversions shown in Figure 6f shows diffuse emissions with a rate of less than 0.002 kg N2O m^{-2} yr^{-1}, representing direct and indirect emissions from fertilized croplands and pastures. There are also hotspots of emissions corresponding to industrial emitters and high emission rates from intensive agriculture over Benelux (0.005 kg N2O m^{-2} yr^{-1}, see de Vries et al. 2021). The trend of N_2O emissions optimized by inversions that will be updated in EYE-CLIMA (Figure 6h) is slightly negative for all diffuse emissions in Germany and France, consistent with reduced nitrogen fertilizers applications (following the Nitrate Directive of the EEC, 1991), whereas prior emissions used by inversions had no trend. On the other hand, point sources show positive or negative trends. Much of the IPPU emissions from nitric acid plants were cut in a similar manner around 2010, with the introduction of the European Emission Trading System that made it economically interesting for companies to apply emission abatement technologies (catalytic reduction of N_2O in the flue gas) to reduce their emissions (Petrescu et al., 2023). Belgium and the Netherlands indicate a strong increase in N_2O emissions (Figure 6h).

5. Interannual variability of European GHG budgets

Quantifying interannual variability (IAV) and identifying its drivers is important to gain understanding of the processes controlling variations in sources and sinks of GHGs, but also to appropriately separate long-term trends (human-driven) from short-lived variations due to natural climate variability. Variability in the European CO_2 sink has been previously analyzed, including the main drivers of long-term IAV in sources and sinks of CO_2 (Ciais et al. 2010; Luyssaert et al., 2010; Bastos et al., 2016), seasonal compensation effects (Buermann et al., 2018) and the impacts of extreme events on annual carbon budgets (Ciais et al., 2005; Bastos et al. 2014; Bastos et al., 2020). For CH_4 and N_2O, less is known about the magnitude and spatiotemporal distribution of IAV in the European region. It is also unclear how IAV

This project has received funding from the European Union's Horizon Europe research and innovation programme under grant agreement No 101081395

in each of the three GHGs relates to variability in the overall global warming potential (GWP). Depending on the main drivers of variability in each GHG, anomalies may reinforce each other in a particular year (if climatic conditions lead to anomalies of the same sign in all three GHGs) or counterbalance each other partly (if the same climatic conditions lead to anomalies of opposite signs among the GHGs). In this section we compare the magnitude and spatial distribution of IAV in net CO_2, CH_4 and N_2O emissions and their combined GWP at the 20-yr and 100-yr time horizons (GWP_{20} and GWP_{100}, respectively). We then analyze how two important modes of climate variability influencing European climate affect anomalies in the three GHGs separately, as well as their combined GWP.

Figure 7 shows the regionally-integrated annual anomalies of CO_2, CH_4 and N_2O and the respective aggregated GWP_{20} and GWP_{100} anomalies from the global atmospheric inversions. For CH_4, we show separately the in-situ and satellite based inversions, due to their different temporal coverage. Both CH_4 and N_2O show a decreasing trend, while CO_2 shows multi-annual variations with a predominant sink in the 1990s and predominant source fluxes in the 2000s. Hot and dry years are generally associated with source anomalies, except 2012 and 2015, when drought conditions were more localized and mostly located over southern Europe. The 2003 drought and the 2018-2020 extreme summers were associated with strong CO_2 sources. 2003 is also associated with large CH_4 and N_2O sources, so that 2003 is the year with the highest associated GWP, and 2010 shows a peak in emissions following a downward trend (bottom panel). It should be noted that the spread of the inversions is generally larger than the anomalies themselves for all three GHGs, which indicates a reduced ability to constrain annual anomalies at continental scale.

This project has received funding from the European Union's Horizon Europe research and innovation programme under grant agreement No 101081395

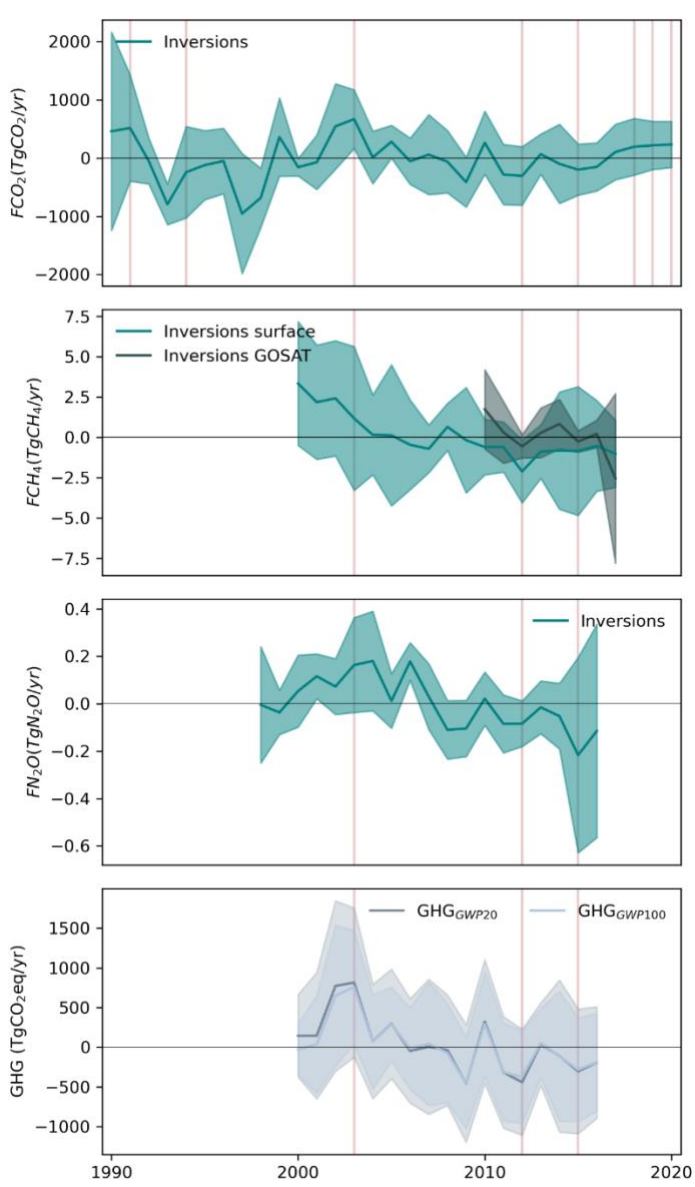

Figure 7. Time-series of annual anomalies of the three GHGs - CO_2, CH_4 and N2O from top to the third panel, and the respective aggregated GWP_{20} and GWP_{100} anomalies. The vertical red lines indicate years associated with hot and/or drought events. This figure is reproduced from Lauerwald et al. 2024.

In Figure 8, we evaluate how anomalies in the three GHGs vary with two important modes of large-scale atmospheric circulation influencing European climate: the North Atlantic Oscillation (NAO) and the East-Atlantic (EA) Pattern. We analyze how far anomalies in each GHG and GWP of all three GHGs combined are related to possible NAO/EA combinations - at European scale, and for four major climate regions within Europe: Atlantic, Continental, Boreal, and Mediterranean. At European scale, we find that both combinations of NAO/EA in-phase (NAO+EA+ and NAO-EA-) are associated with below-average GWP (GHG_{GWP20}). In the case of NAO+EA+, this is because of a combination of below-average values of CO_2 and N2O, but this is likely driven by outlier values, as the median anomalies for both gasses are close to zero. For NAO-EA-, CO_2 anomalies are predominantly negative, consistent with the results in Bastos et al. (2016), along with generally negative CH_4 anomalies, which are however associated with a large spread among inversions. Because the impacts of NAO and EA are regionally different, we need to analyze the regional dependence of GHG anomalies on climate drivers for each NAO/EA phase. During NAO+EA+, GHG sink anomalies are found for all regions except the Atlantic sector, but this is due to

This project has received funding from the European Union's Horizon Europe research and innovation programme under grant agreement No 101081395

different combinations of anomalies in the three GHGs and of climate conditions: below-average GHG emissions in Continental and Boreal regions are mainly associated with below-average CO_2 anomalies driven by warmer than average conditions and close to normal - but slightly negative - precipitation anomalies. In the Atlantic section, warmer and drier conditions during NAO+EA+ are associated with a positive CO_2 anomaly, which is partly offset by a negative N_2O anomaly, consistent with below average precipitation. For NAO-EA-, the European GHG sink is dominated by negative GHG_{GWP20} anomalies in Continental and Mediterranean regions, mostly associated with below-average CO_2 emissions in both regions and additionally with negative CH_4 anomalies in the Mediterranean. In the Boreal section, negative CO_2 anomalies are linked to below average temperature and precipitation, consistent with results in Bastos et al. (2016) who showed that increased snow cover in winter due to cold winters and later soil-moisture availability led to increased summer GPP, while predominantly cooler temperatures keeping Re_{terr} anomalies low. The above-average N_2O emissions in this region might be associated with the higher soil moisture during summer in this region (see Bastos et al. (2016) for seasonal climate anomalies). The negative anomalies in GHG_{GWP20} in the Mediterranean are also likely explained by differences in the seasonal climate anomalies, with the increased CO_2 sink associated with higher soil-moisture availability during winter and early spring, when vegetation activity is at its peak in this region.

For the anti-phase combinations, GHG_{GWP20} shows a clear source anomaly for NAO-EA+ and close to neutral but predominantly source anomaly for NAO+EA-, with both phase combinations showing a very large spread (Figure 8). The clear GHG_{GWP20} source anomaly in NAO-EA+ results from positive anomalies in the three GHGs at European scale, while NAO+EA- shows close to neutral anomalies for all three GHGs, although slightly positive for CO_2 and slightly negative for CH_4 and N_2O. The continental scale neutral balance for NAO+EA- is explained by offsetting effects between the Boreal and Mediterranean sectors, the first showing a sink anomaly associated with below-average CO_2 and CH_4 along with close to normal but tendentially warmer and slightly wetter than average conditions. Bastos et al. (2016) showed that the warm conditions for this phase occurred predominantly in winter and spring, so that the CO_2 sink might be associated with earlier onset of the growing season. The positive GHG_{GWP20} anomalies during NAO+EA- in the Mediterranean are associated with CO_2 source anomaly due to lower than average temperatures (especially in winter, the peak of the growing season, see Bastos et al. (2016)) and a N_2O source anomaly likely explained by wetter than average conditions during this phase. Finally, the source anomaly at European scale during NAO-EA+ is mostly explained by positive anomalies in CO_2 and CH_4 in the Continental region, associated with cooler than average and much wetter conditions, and by positive anomalies in all three GHGs in the Atlantic region, associated with warmer and wetter conditions during this phase.

This project has received funding from the European Union's Horizon Europe research and innovation programme under grant agreement No 101081395

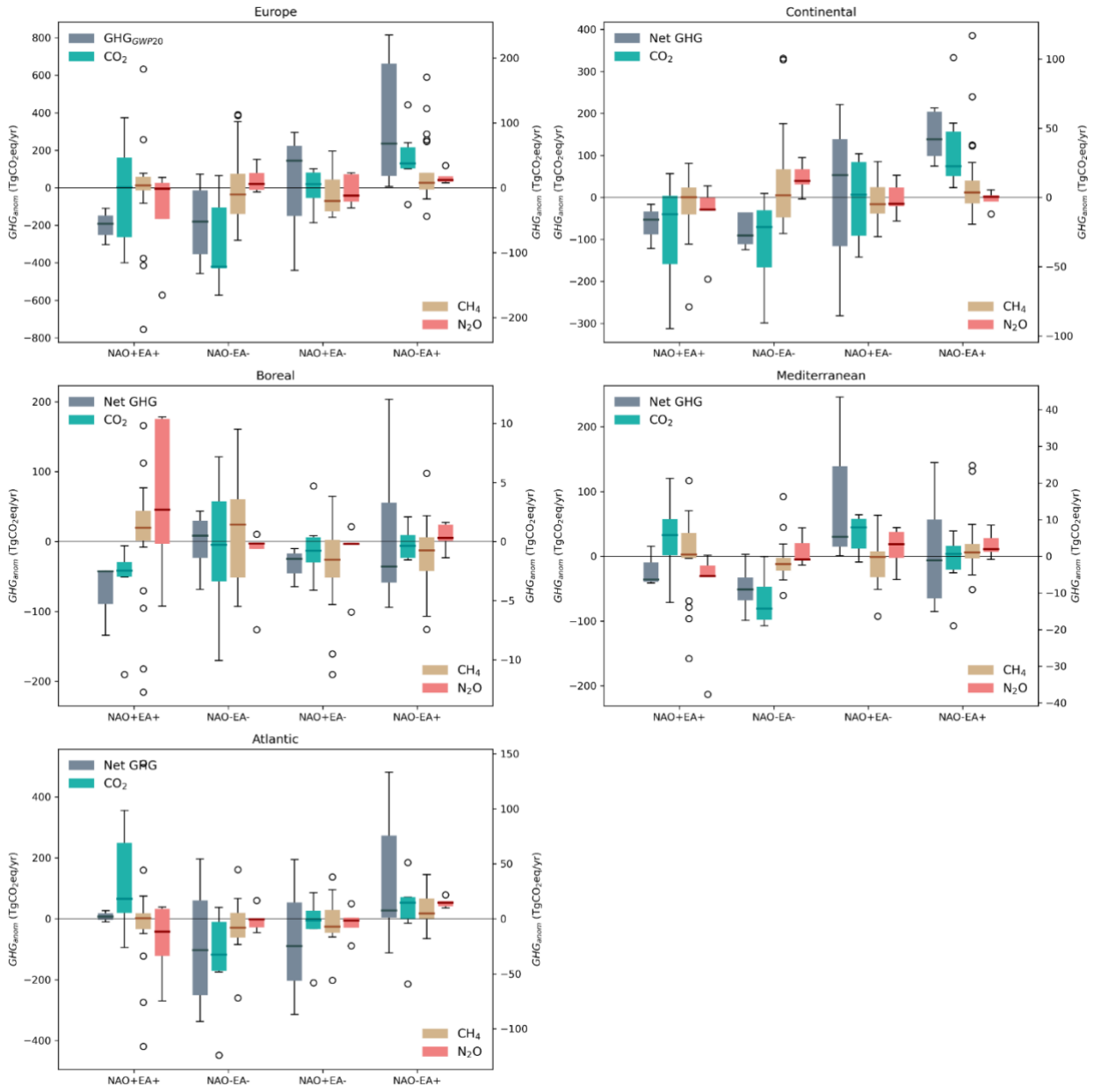

Figure 8. Anomalies in annual CO_2, CH_4 and N2O fluxes and combined GWP_{20} during the four combined phases of two main atmospheric circulation patterns influencing European climate: the North Atlantic Oscillation (NAO) and the East Atlantic Pattern (EA). The boxplots show the spread across the inversions for the mean of each phase combination. For each individual GHG, the anomalies are calculated for the available time-series length for each GHG, while for the GWP, the data are limited to the period 2000-2016, so that only two years are considered for the two in-phase composites (NAO+EA+ and NAO-EA-). This figure is reproduced from Lauerwald et al. 2024.

6. Conclusion

The EYE-CLIMA project supported this synthesis for the update of a CO_2 inversion and the support for the GAINS inventory for N_2O and CH_4 anthropogenic emissions. New inversions at higher resolution than used in this study are under preparation in EYE-CLIMA and will provide more detail on the spatial and temporal distributions of the fluxes for the next synthesis. The data analytics framework proposed in this study and used by Lauerwald et al. was supported by EYE-CLIMA as the VERFY project terminated before the start of this study.

This project has received funding from the European Union's Horizon Europe research and innovation programme under grant agreement No 101081395

The BU estimate of the European greenhouse gas (GHG) budget for the decade 2010-2019 indicates net emissions of 3.9 Pg CO_2-eq.yr^{-1}over a 100-year horizon. These emissions are driven by direct anthropogenic sources, amounting to 4.9 Pg CO_2-eq.yr^{-1}, with fossil fuel combustion from the Energy and IPPU sectors contributing approximately 85%. The land GHG budget demonstrates a net sink of 0.9 Pg CO_2-eq.yr^{-1}, predominantly due to a land CO_2 sink of 1.4 Pg CO_2-eq.yr^{-1}, partially offset by net emissions of CH_4 and N_2O. Our BU CH_4 and N_2O budgets align closely with regional and global inversion estimates. However, our BU estimate of the land CO_2 sink is at the upper end of global inversion estimates and significantly higher than regional inversion estimates. Across the 1990s, 2000s, and 2010s, BU estimates indicate a declining trend in average net GHG emissions (anthropogenic emissions + land budget) of 5.1 Pg CO_2-eq.yr^{-1}, 4.6 Pg CO_2-eq.yr^{-1}, and 3.9 Pg CO_2-eq.yr^{-1}, respectively. This reduction is mainly driven by decreases in direct anthropogenic emissions of CO_2 and CH_4, particularly due to a significant reduction in fossil fuel emissions from the 2000s to the 2010s by 0.7 Pg CO_2 yr^{-1}. This reduction was partially offset by a weakening of the land CO_2 sink by 0.2 Pg CO_2 yr^{-1}. N_2O emissions contribute less to the overall GHG budget but also show a significant decrease, largely due to reduced emissions from the IPPU sector, though considerable uncertainties remain.

TD estimates, derived from global inversions covering the last two to three decades, corroborate the decreasing trend in CH_4 and N_2O emissions. For the land CO_2 budget, the trend is less clear, with significant interannual variability. Extreme weather events, such as the drought of 2003 and the hot summers of 2018 and 2020, have likely contributed to a weakened land CO_2 sink during these years. The 2003 drought also resulted in the highest net GHG emissions in terms of the combined global warming potential of the three GHGs. Regional inversions reveal large-scale spatial patterns of GHG emissions across Europe. CO_2 emissions from anthropogenic sources, particularly fossil fuels, are concentrated in local hotspots associated with large cities, power plants, and industrial complexes. For the land CO2 budget, regional inversions identify sinks mainly in northern Europe, whereas southern France and the Iberian Peninsula act as significant CO_2 sources. CH_4 and N_2O emissions are predominantly from diffuse agricultural sources, with notable hotspots in Belgium, the Netherlands, and southern UK due to intensive agricultural activities.

Overall, this deliverable provides the most comprehensive and up-to-date assessment of the European CO_2, CH_4, and N_2O budgets over the past three decades, including their combined global warming potential, trends, and interannual variability. By integrating a broad range of BU and TD estimates, we have disaggregated these budgets into their constituent components, offering a robust estimate for the 2010s. This study, in comparison with UNFCCC reports, offers crucial insights for the independent verification of regional climate change mitigation progress and supports the development of a European-scale carbon monitoring framework to inform policy-making.

7. References

Ahlström, A., Canadell, J. G., & Metcalfe, D. B. (2022). Widespread Unquantified Conversion of Old Boreal Forests to Plantations. Earth's Future, 10(11), e2022EF003221. https://doi.org/10.1029/2022EF003221

Bastos, A., Gouveia, C. M., Trigo, R. M., & Running, S. W. (2014). Analysing the spatio-temporal impacts of the 2003 and 2010 extreme heatwaves on plant productivity in Europe. Biogeosciences, 11(13), 3421–3435. https://doi.org/10.5194/bg-11-3421-2014

Bastos, A., Fu, Z., Ciais, P., Friedlingstein, P., Sitch, S., Pongratz, J., et al. (2020). Impacts of extreme summers on European ecosystems: A comparative analysis of 2003, 2010 and 2018: European extreme

This project has received funding from the European Union's Horizon Europe research and innovation programme under grant agreement No 101081395

summers and the C-cycle. Philosophical Transactions of the Royal Society B: Biological Sciences, 375(1810). https://doi.org/10.1098/rstb.2019.0507

Bastos, Ana, Janssens, I. A., Gouveia, C. M., Trigo, R. M., Ciais, P., Chevallier, F., et al. (2016). European land CO2 sink influenced by NAO and East-Atlantic Pattern coupling. Nature Communications, 7(1), 10315. https://doi.org/10.1038/ncomms10315

Battin, T. J., Lauerwald, R., Bernhardt, E. S., Bertuzzo, E., Gener, L. G., Hall, R. O., et al. (2023). River ecosystem metabolism and carbon biogeochemistry in a changing world. Nature, 613(7944), 449–459. https://doi.org/10.1038/s41586-022-05500-8

Buermann, W., Forkel, M., O'Sullivan, M., Sitch, S., Friedlingstein, P., Haverd, V., et al. (2018). Widespread seasonal compensation effects of spring warming on northern plant productivity. Nature, 562(7725), 110–114. https://doi.org/10.1038/s41586-018-0555-7

Chang, J., Ciais, P., Gasser, T., Smith, P., Herrero, M., Havlík, P., et al. (2021). Climate warming from managed grasslands cancels the cooling effect of carbon sinks in sparsely grazed and natural grasslands. Nature Communications, 12(1), 118. https://doi.org/10.1038/s41467-020-20406-7

Ciais, P., Soussana, J. F., Vuichard, N., Luyssaert, S., Don, A., Janssens, I. A., et al. (2010). The greenhouse gas balance of European grasslands. Biogeosciences Discuss., 2010, 5997–6050. https://doi.org/10.5194/bgd-7-5997-2010

Ciais, P., Yao, Y., Gasser, T., Baccini, A., Wang, Y., Lauerwald, R., et al. (2021). Empirical estimates of regional carbon budgets imply reduced global soil heterotrophic respiration. National Science Review, 8(2). https://doi.org/10.1093/nsr/nwaa145

Ciais, P., Bastos, A., Chevallier, F., Lauerwald, R., Poulter, B., Canadell, J. G., et al. (2022). Definitions and methods to estimate regional land carbon fluxes for the second phase of the REgional Carbon Cycle Assessment and Processes Project (RECCAP-2). Geoscientific Model Development, 15(3), 1289–1316. https://doi.org/10.5194/gmd-15-1289-2022

Ciais, Ph, Reichstein, M., Viovy, N., Granier, A., Ogée, J., Allard, V., et al. (2005). Europe-wide reduction in primary productivity caused by the heat and drought in 2003. Nature, 437(7058), 529–533. https://doi.org/10.1038/nature03972

Deng, Z., Ciais, P., Tzompa-Sosa, Z. A., Saunois, M., Qiu, C., Tan, C., et al. (2022). Comparing national greenhouse gas budgets reported in UNFCCC inventories against atmospheric inversions. Earth System Science Data, 14(4), 1639–1675. https://doi.org/10.5194/essd-14-1639-2022

Etiope, G., Ciotoli, G., Schwietzke, S., & Schoell, M. (2019). Gridded maps of geological methane emissions and their isotopic signature. Earth System Science Data, 11(1), 1–22. https://doi.org/10.5194/essd-11-1-2019

Friedlingstein, P., Jones, M. W., O'Sullivan, M., Andrew, R. M., Bakker, D. C. E., Hauck, J., et al. (2022). Global Carbon Budget 2021. Earth System Science Data, 14(4), 1917–2005. https://doi.org/10.5194/essd-14-1917-2022

Guimberteau, M., Zhu, D., Maignan, F., Huang, Y., Yue, C., Dantec-Nédélec, S., et al. (2018). ORCHIDEE-MICT (v8.4.1), a land surface model for the high latitudes: model description and validation. Geoscientific Model Development, 11(1), 121–163. https://doi.org/10.5194/gmd-11-121-2018

This project has received funding from the European Union's Horizon Europe research and innovation programme under grant agreement No 101081395

Hartmann, J., Jansen, N., Dürr, H. H., Kempe, S., & Köhler, P. (2009). Global CO2-consumption by chemical weathering: What is the contribution of highly active weathering regions? Global and Planetary Change, 69(4), 185–194. https://doi.org/10.1016/j.gloplacha.2009.07.007

Hersbach, H., Bell, B., Berrisford, P., Hirahara, S., Horányi, A., Muñoz-Sabater, J., et al. (2020). The ERA5 global reanalysis. Quarterly Journal of the Royal Meteorological Society, 146(730), 1999–2049. https://doi.org/10.1002/qj.3803

Jung, M., Schwalm, C., Migliavacca, M., Walther, S., Camps-Valls, G., Koirala, S., et al. (2020). Scaling carbon fluxes from eddy covariance sites to globe: synthesis and evaluation of the FLUXCOM approach. Biogeosciences, 17(5), 1343–1365. https://doi.org/10.5194/bg-17-1343-2020

Kaiser, J. W., Heil, A., Andreae, M. O., Benedetti, A., Chubarova, N., Jones, L., et al. (2012). Biomass burning emissions estimated with a global fire assimilation system based on observed fire radiative power. Biogeosciences, 9(1), 527–554. https://doi.org/10.5194/bg-9-527-2012

Lauerwald, R., Allen, G. H., Deemer, B. R., Liu, S., Maavara, T., Raymond, P., et al. (2023). Inland Water Greenhouse Gas Budgets for RECCAP2: 2. Regionalization and Homogenization of Estimates. Global Biogeochemical Cycles, 37(5). https://doi.org/10.1029/2022GB007658

Li, N., Sippel, S., Winkler, A. J., Mahecha, M. D., Reichstein, M., & Bastos, A. (2022). Interannual global carbon cycle variations linked to atmospheric circulation variability. Earth System Dynamics, 13(4), 1505–1533. https://doi.org/10.5194/esd-13-1505-2022

Luyssaert, S., Ciais, P., Piao, S. L., Schulze, E.-D., Jung, M., Zaehle, S., et al. (2010). The European carbon balance. Part 3: forests. Global Change Biology, 16(5), 1429–1450. https://doi.org/10.1111/j.1365-2486.2009.02056.x

Luyssaert, S., Abril, G., Andres, R., Bastviken, D., Bellassen, V., Bergamaschi, P., et al. (2012). The European land and inland water CO2, CO, CH4 and N2O balance between 2001 and 2005. Biogeosciences, 9(8), 3357–3380. https://doi.org/10.5194/bg-9-3357-2012.

Lauerwald, R., A.Bastos, M.J. McGrath, A.M.R. Petrescu, F. Ritter, R.M. Andrew, A. Berchet, G. Broquet, D. Brunner, F. Chevallier, A. Cescatti, S. Filipek, A. Fortems-Cheiney, G. Forzieri, P. Friedlingstein, R. Fuchs, C. Gerbig, S. Houweling, P. Ke, B.J.W. Lerink, W. Li, X. Li, I.T. Luijkx, G. Monteil, S. Munassar, G.-J. Nabuurs, P.K. Patra, P. Peylin, J. Pongratz, P. Regnier, M. Saunois, M.-J. Schelhaas, M. Scholze, S. Sitch, R.L. Thompson, H. Tian, A. Tsuruta, C. Wilson, J.-P. Wigneron, Y. Yao, S. Zaehle, , W. Li, and P. Ciais 2024. Carbon and greenhouse gas budgets of Europe: trends, interannual and spatial variability, and their drivers. Paper submitted to Global Biogeochem Cycles, 2024. https://doi.org/10.22541/essoar.171320253.37867733/v1.

Madani, N., Parazoo, N.C. (2020). Global Monthly GPP from an Improved Light Use Efficiency Model, 1982-2016. ORNL DAAC, Oak Ridge, Tennessee, USA. https://doi.org/10.3334/ORNLDAAC/1789

McGrath, M. J., Petrescu, A. M. R., Peylin, P., Andrew, R. M., Matthews, B., Dentener, F., et al. (2023). The consolidated European synthesis of CO2 emissions and removals for the European Union and United Kingdom: 1990-2020. Earth System Science Data, 15(10), 4295–4370. https://doi.org/10.5194/essd-15-4295-2023

Meybeck, M., Dürr, H. H., & Vörösmarty, C. J. (2006). Global coastal segmentation and its river catchment contributors: A new look at land-ocean linkage. Global Biogeochemical Cycles, 20(1). https://doi.org/10.1029/2005GB002540

This project has received funding from the European Union's Horizon Europe research and innovation programme under grant agreement No 101081395

Monteil, G., Broquet, G., Scholze, M., Lang, M., Karstens, U., Gerbig, C., et al. (2020). The regional European atmospheric transport inversion comparison, EUROCOM: first results on European-wide terrestrial carbon fluxes for the period 2006–2015. Atmospheric Chemistry and Physics, 20(20), 12063–12091. https://doi.org/10.5194/acp-20-12063-2020

Moran, D., Pichler, P.-P., Zheng, H., Muri, H., Klenner, J., Kramel, D., et al. (2022). Estimating CO_2 emissions for 108000 European cities. Earth System Science Data, 14(2), 845–864. https://doi.org/10.5194/essd-14-845-2022

Murguia-Flores, F., Arndt, S., Ganesan, A. L., Murray-Tortarolo, G., & Hornibrook, E. R. C. (2018). Soil Methanotrophy Model (MeMo v1.0): a process-based model to quantify global uptake of atmospheric methane by soil. Geoscientific Model Development, 11(6), 2009–2032. https://doi.org/10.5194/gmd-11-2009-2018

Petrescu, A. M. R., Qiu, C., Ciais, P., Thompson, R. L., Peylin, P., McGrath, M. J., et al. (2021). The consolidated European synthesis of CH4 and N2O emissions for the European Union and United Kingdom: 1990–2017 Earth System Science Data, 13(5), 2307–2362. https://doi.org/10.5194/essd-13-2307-2021

Petrescu, A. M. R., McGrath, M. J., Andrew, R. M., Peylin, P., Peters, G. P., Ciais, P., et al. (2021). The consolidated European synthesis of CO2 emissions and removals for the European Union and United Kingdom: 1990-2018. Earth System Science Data, 13(5), 2363–2406. https://doi.org/10.5194/essd-13-2363-2021

Petrescu, A. M. R., Qiu, C., McGrath, M. J., Peylin, P., Peters, G. P., Ciais, P., et al. (2023). The consolidated European synthesis of CH4 and N2O emissions for the European Union and United Kingdom: 1990-2019. Earth System Science Data, 15(3), 1197–1268. https://doi.org/10.5194/essd-15-1197-2023

Rosentreter, J. A., Laruelle, G. G., Bange, H. W., Bianchi, T. S., Busecke, J. J. M., Cai, W.-J., et al. (2023). Coastal vegetation and estuaries are collectively a greenhouse gas sink. Nature Climate Change, 13(6), 579–587. https://doi.org/10.1038/s41558-023-01682-9

Saunois, M., Stavert, A. R., Poulter, B., Bousquet, P., Canadell, J. G., Jackson, R. B., et al. (2020). The Global Methane Budget 2000–2017. Earth System Science Data, 12(3), 1561–1623. https://doi.org/10.5194/essd-12-1561-2020

Solazzo, E., Crippa, M., Guizzardi, D., Muntean, M., Choulga, M., & Janssens-Maenhout, G. (2021). Uncertainties in the Emissions Database for Global Atmospheric Research (EDGAR) emission inventory of greenhouse gases. Atmospheric Chemistry and Physics, 21(7), 5655–5683. https://doi.org/10.5194/acp-21-5655-2021

Tian, H., Yang, J., Xu, R., Lu, C., Canadell, J. G., Davidson, E. A., et al. (2019). Global soil nitrous oxide emissions since the preindustrial era estimated by an ensemble of terrestrial biosphere models: Magnitude, attribution, and uncertainty. Global Change Biology, 25(2), 640–659. https://doi.org/10.1111/gcb.14514

Tian, H., Xu, R., Canadell, J. G., Thompson, R. L., Winiwarter, W., Suntharalingam, P., et al. (2020). A comprehensive quantification of global nitrous oxide sources and sinks. Nature, 586(7828), 248–256. https://doi.org/10.1038/s41586-020-2780-0

This project has received funding from the European Union's Horizon Europe research and innovation programme under grant agreement No 101081395

Tian, Hanqin, Lu, C., Ciais, P., Michalak, A. M., Canadell, J. G., Saikawa, E., et al. (2016). The terrestrial biosphere as a net source of greenhouse gases to the atmosphere. Nature, 531(7593), 225–228. https://doi.org/10.1038/nature16946

Tubiello, F. N., Salvatore, M., Rossi, S., Ferrara, A., Fitton, N., & Smith, P. (2013). The FAOSTAT database of greenhouse gas emissions from agriculture. Environmental Research Letters, 8(1). https://doi.org/10.1088/1748-9326/8/1/015009

Velthof, G. L., Lesschen, J. P., Webb, J., Pietrzak, S., Miatkowski, Z., Pinto, M., et al. (2014). The impact of the Nitrates Directive on nitrogen emissions from agriculture in the EU-27 during 2000–2008. Science of The Total Environment, 468–469, 1225–1233. https://doi.org/10.1016/j.scitotenv.2013.04.058

de Vries, W., Schulte-Uebbing, L., Kros, H., Voogd, J. C., & Louwagie, G. (2021). Spatially explicit boundaries for agricultural nitrogen inputs in the European Union to meet air and water quality targets. Science of The Total Environment, 786, 147283. https://doi.org/10.1016/j.scitotenv.2021.147283

Winkler, K., Fuchs, R., Rounsevell, M., & Herold, M. (2021). Global land use changes are four times greater than previously estimated. Nature Communications, 12(1), 2501. https://doi.org/10.1038/s41467-021-22702-2

Winkler, K., Yang, H., Ganzenmüller, R., Fuchs, R., Ceccherini, G., Duveiller, G., et al. (2023). Changes in land use and management led to a decline in Eastern Europe's terrestrial carbon sink. Communications Earth & Environment, 4(1), 237. https://doi.org/10.1038/s43247-023-00893-4

Yao, Yitong, Ciais, P., Viovy, N., Li, W., Cresto-Aleina, F., Yang, H., et al. (2021). A Data-Driven Global Soil Heterotrophic Respiration Dataset and the Drivers of Its Inter-Annual Variability. Global Biogeochemical Cycles, 35(8), e2020GB006918. https://doi.org/10.1029/2020GB006918

Yao, Yuanzhi, Tian, H., Shi, H., Pan, S., Xu, R., Pan, N., & Canadell, J. G. (2020). Increased global nitrous oxide emissions from streams and rivers in the Anthropocene. Nature Climate Change, 10(2), 138–142. https://doi.org/10.1038/s41558-019-0665-8

Zhao, M., Heinsch, F. A., Nemani, R. R., & Running, S. W. (2005). Improvements of the MODIS terrestrial gross and net primary production global data set. Remote Sensing of Environment, 95(2), 164–176. https://doi.org/10.1016/j.rse.2004.12.011

Zscheischler, J., Mahecha, M. D., Avitabile, V., Calle, L., Carvalhais, N., Ciais, P., et al. (2017). Reviews and syntheses: An empirical spatiotemporal description of the global surface-atmosphere carbon fluxes: Opportunities and data limitations. Biogeosciences, 14(15), 3685–3703. https://doi.org/10.5194/bg-14-3685-2017

This project has received funding from the European Union's Horizon Europe research and innovation programme under grant agreement No 101081395

https://eyeclima.eu

BRUSSELS, 27 08 2024

Funded by the European Union. Views and opinions expressed are however those of the author(s) only and do not necessarily reflect those of the European Union. Neither the European Union nor the granting authority can be held responsible for them.

This project has received funding from the European Union's Horizon Europe research and innovation programme under grant agreement No 101081395